JOURNAL OF GEOPHYSICAL RESEARCH, VOL. 103, NO. D11, PAGES 13,413–13,434, JUNE 20, 1998

Chemical air mass differences near fronts

S. Bethan and G. Vaughan

Department of Physics, University of Wales, Aberystwyth, U.K.

C. Gerbig and A. Volz-Thomas

Institut fur Chemie und Dynamik der Geosphäre (ICG-2), Forschungszentrum Jülich, Germany

H. Richer and D. A. Tiddeman

Meteorological Research Flight, U.K. Meteorological Office, Hampshire, U.K.

Abstract. Two case studies are presented of aircraft measurements (ozone, NO_y, CO, and meteorological parameters) in the vicinity of fronts located over the eastern side of the North Atlantic Ocean during spring 1994. The aim of these studies was twofold: (1) to investigate whether frontal circulations can transport ozone from the boundary layer to the free troposphere in well-defined layer; and (2) to ascertain whether or not conveyor belts associated with extratropical cyclones exhibit well-defined chemical signatures. The first case study (March 2, 1994) sampled a well-defined ozone-enhanced layer within the free troposphere. It is demonstrated that this air was transferred from the boundary layer to the free troposphere during the development of a baroclinic wave. Two warm conveyor belts sampled within this flight (one associated with the developing baroclinic wave and the other with a mature low-pressure system) displayed clear and contrasting chemical signatures, a consequence of their geographically different origins. During the second case study (April 25, 1994), both the dry intrusion and the warm conveyor belt of a mature, occluded low-pressure system were sampled. Their chemical signatures (in particular, that of the dry intrusion) showed that interleaving of the two airstreams had occurred, probably in the vicinity of the occluded front. It is thus demonstrated that chemical measurements within conveyor belts provide valuable information on the nature, history, and extent of these coherent flows.

1. Introduction

Despite the fact that only approximately 10% of the total atmospheric ozone is found in the free troposphere, it has a crucial role to play in tropospheric photochemistry. Ozone is the primary source of the hydroxyl radical (OH) which is produced when ozone is photolyzed by UV radiation in the presence of water vapor; OH is responsible for the removal of carbon monoxide, methane [*Levy*, 1971], nitrogen dioxide, and hydrocarbons from the atmosphere. By absorption of thermal radiation at 9.6 μm, ozone also plays an important role in the energy budget of the troposphere [*Ramanathan and Dickinson*, 1979; *Fishman et al.*, 1979].

The ozone content of the free troposphere is determined by the combination of in situ photochemistry and transport to and from the stratosphere and boundary layer. The stratosphere is characterized by very dry air low in CO and hydrocarbons and rich in ozone and NO_y (which are closely correlated [*Murphy et al.*, 1993; *Fahey et al.*, 1996]. Stratospheric intrusions into the troposphere are therefore fairly readily identified in tracer measurements; for example, they appear in ozonesonde profiles as dry, ozone-rich layers of high static stability [*Beekmann et al.*, 1994], although because of mixing with surrounding tropospheric air, the characteristic stratospheric ratio between constituents such as ozone and NO_y is not conserved. The marine boundary layer is generally poor in CO, O_3, and NO_y with high humidity, whereas polluted continental boundary layer air is generally humid with high CO and hydrocarbon concentrations. The ozone and NO_y content of continental boundary layer air is extremely variable, both in location and season, and depends on the efficacy of photochemical and deposition processes. There is no unique chemical signature therefore of air recently transported from the boundary layer to the free troposphere. However, this paper aims to show that by a combination of chemical measurements and meteorological analyses such transport can be identified, so that eventually an estimate of the contribution of the boundary layer source to the ozone content of the free troposphere may be obtained.

The processes responsible for transferring air from the stratosphere to the troposphere are reasonably well

Paper number 98JD00535.
0148-0227/98/98JD-00535$09.00

understood [*Holton et al.*, 1995]; however, comparatively little is known about the transfer of pollutants from the boundary layer to the free troposphere. The focus of most such studies has been on transport in convective clouds [e.g., *Pickering et al.*, 1988, 1996; *Cho et al.*, 1989; *Ritter*, 1984; *Chatfield and Crutzen*, 1984; *Niewiadomski*, 1986], although frontal systems have also been recognized as an important mechanism in the vertical redistribution of pollutants [*Brown et al.*, 1984; *Banic et al.*, 1986; *Kavassalis et al.*, 1986; *Chaumerliac et al.*, 1992; *Gimson*, 1994]. Such processes can influence the ozone budget of the free troposphere directly by transferring ozone upward from a polluted boundary layer, or indirectly by transporting chemical precursors. The local chemical budget of ozone is a nonlinear function of the mixing ratios of H_2O, NO_y (and its partitioning between NO_x and other compounds such as HNO_3, HNO_4, or PAN), and ozone itself as well as the UV radiation field. Recycling of NO_x from HNO_3 is more effective in the upper troposphere, and NO_x can be recycled during subsidence from thermally unstable compounds such as PAN and HNO_4. Note, however, that the mixing associated with vertical transport in the atmosphere dilutes NO_y mixing ratios well below the concentrations found in the polluted boundary layer [*Wild et al.*, 1996]. Additional reduction of NO_y occurs by washout of, for example, HNO_3. Finally, H_2O mixing ratios decrease substantially with altitude, so that both the production and destruction rates of ozone in the free troposphere are considerably less than in the sunlit polluted boundary layer.

The majority of extant studies on the role of fronts in transporting pollutants either concentrate on their contribution to acid deposition [e.g., *Hegg et al.*, 1984; *Kavassalis et al.*, 1986] and/or are modeling studies [e.g., *Chaumerliac et al.*, 1992; *Gimson*, 1994]. Analysis of airflow trajectories through midlatitude systems [e.g., *Browning and Pardoe*, 1973; *Browning and Monk*, 1982; *Browning*, 1990; *Browning and Roberts*, 1994; *Browning and Golding*, 1995; *Harrold*, 1973; *Carlson*, 1980] has shown that when air motion is considered relative to the movement of the front or cyclone (relative wind isentropic flow), sharply defined boundaries emerge which differentiate airstreams of vastly differing moisture content; that is, motions associated with midlatitude cyclones form well-defined concentrated flows (Figure 1). These airstreams tend to contain relatively narrow ranges of potential temperature and wet-bulb potential temperature, θ_w, peculiar to the airstreams' origins and are termed conveyor belts. θ_w is defined as the temperature attained by displacing a parcel of air from its local condensation level to 1000 mbar along a saturated adiabatic curve on a thermodynamic diagram such as a tephigram [*Wallace and Hobbs*, 1977, p.79]. It is conserved when an air parcel is displaced adiabatically, irrespective of whether or not it is saturated. *Sturman and McGowan* [1995] found θ_w to be a more successful indicator of the geographical origin of boundary layer air than equivalent potential temperature, virtual potential temperature, or relative humidity, and it is commonly used in identifying three-dimensional airflows associated with fronts and extratropical cyclones [e.g., *Browning and Hill*, 1985; *Browning and Roberts*, 1994; *Browning and Golding*, 1995].

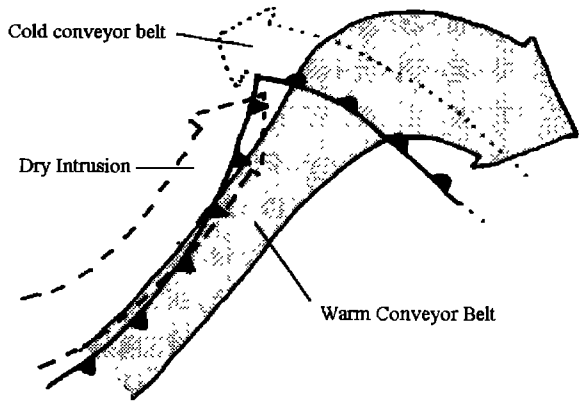

Figure 1. Schematic diagram of relative isentropic flow in a midlatitude cyclone [after *Browning*, 1990]. The warm conveyor belt (stippled) rises from low level at bottom left to the upper troposphere ahead of the warm front. The cold conveyor belt rises more gently, beneath the warm front. After emerging poleward of the WCB, it can turn clockwise or anticlockwise depending on the development of the cyclone. The dry intrusion comprises descending upper tropospheric or stratospheric air.

Three major airflows are associated with a mature cyclone [e.g., *Carlson*, 1980]: the warm conveyor belt (WCB), the cold conveyor belt (CCB), and the dry airstream or intrusion. Their characteristics are described here briefly in terms of flow with respect to the cyclone center (relative isentropic coordinates); for further details, see *Carlson* [1980] and *Browning* [1990]. The WCB is a stream of air with high θ_w that commences in the boundary layer equatorward of the cyclone, travels rapidly along and ahead of a cold front, and ascends while turning anticyclonically above the warm front (if present). The CCB begins at low level ahead of the warm front. It proceeds westward (relative to the cyclone) toward the cyclone center, usually ascending as it travels, such that it is located in the middle troposphere near the apex of the warm sector. Note that it undercuts the WCB such that the warm frontal zone corresponds to the interface between the WCB and CCB. The dry intrusion constitutes air descending from the upper troposphere or lower stratosphere behind the cold front; it can either undercut or overrun the WCB in the vicinity of the cold frontal zone. Recent work [*Wernli and Davies*, 1997; *Wernli*, 1997] involving a Lagrangian-based analysis scheme to identify coherent ensembles of trajectories (CETs) that accompany Atlantic cyclogenesis has confirmed the existence of several distinct quasi-continuous moist ascending (and dry descending) CETs. Clearly, the flows that originate within the boundary layer and ascend into the free troposphere have considerable potential for transferring trace gases between these two regions.

In this paper, two case studies are presented of aircraft measurements (of both soluble and insoluble trace gases) through fronts located to the southwest of the United Kingdom during spring 1994. The aims of the study are twofold: (1) to investigate whether circulations associated with fronts can transport significant quantities of ozone and precursors from the boundary layer into the free troposphere in well-defined layers and (2) to ascertain whether or not conveyor belts associated with extratropical cyclones are delineated by well-defined chemical signatures. Can these flows therefore explain variations in observed trace gas distributions?

The first case study (section 3) presents measurements through a developing baroclinic wave on the polar front over the eastern Atlantic, while the second (section 4) presents measurements through a well-developed warm front associated with a mature low-pressure system to the west of Ireland. Both cases were of particular interest because of the presence of elevated ozone concentrations ahead of (i.e., below) the warm frontal surface. This is surprising given that the transfer of stratospheric air associated with an extra-tropical cyclone occurs behind the cold front and that the major flow of air from the boundary layer to the free troposphere (the WCB) occurs to the rear of the warm frontal surface.

Both studies commence with a presentation of the synoptic situation at the time of the measurements; radiosonde profiles along with aircraft measurements in the region of study follow. Finally, the histories of the air masses sampled are investigated with the aid of satellite images, back trajectories, and numerical model output. Conclusions drawn, including answers to the above questions, are presented in section 5.

2. Aircraft Instrumentation

Aircraft measurements presented here were obtained by the U.K. Meteorological Office's C-130 Hercules during the Oxidizing Capacity of the Tropospheric Atmosphere (OCTA) campaigns in March and April 1994. An overall description of the aircraft instrumentation is given by *Nicholls* [1978]. CO was measured using a novel resonance fluorescence instrument (*Gerbig et al.*, 1996), which achieved a precision of 2.5 ppbv for an integration time of 9 s, as was used in the present study. NO_y was measured with a chemiluminescence detector following the conversion of the different NO_x species to NO in a gold tube at 300°C in the presence of CO (0.1%). The converter was operated at a constant pressure of 200 mbar and at a constant flow rate of 1 standard liter per minute (SLpm). The instrument was calibrated before, during, and after the flights with a standard mixture of NO. The conversion efficiency was checked with NO_2 produced by gas phase titration of NO and with HNO_3 from a calibrated permeation tube. The inlet tube (1/4" Teflon tube, 80 cm long) was heated to 30°C in order to reduce inlet losses for HNO_3 to less than 30% for moist planetary boundary layer (PBL) air and to less than 10% for measurements in the free troposphere. The precision (from counting statistics) was 10 parts per trillion by volume (pptv) for 1 min averages. The detection limit of the NO_x measurement as estimated from background variations was 150 pptv. The systematic errors from the background do not affect the conclusions of this study, which is mainly concerned with relative changes in NO_y. NO was also measured using chemiluminescence with a precision of 10 pptv for 1 min averages. For an integration time of 9 s, as used here, NO mixing ratios were mostly in the range of the detection limit (20 pptv). Therefore the NO data are not shown in the figures but are discussed in those cases when enhanced NO mixing ratios were found. Intercomparison with the National Oceanic and Atmospheric Administration (NOAA) instrument aboard the National Center for Atmospheric Research (NCAR) King Air showed agreement for NO and NO_y within the estimated errors. A Bendix 5000 chemiluminescent analyzer provided measurements of ozone with time resolution 15 s and precision 1 ppbv. Bottle samples were taken on board the aircraft for later chromatographic analysis for hydrocarbons, halocarbons, and N_2O, as described by *McKenna et al.* [1995].

Temperature was measured by a Rosemount platinum resistance thermometer to an accuracy of ± 0.3% with dew point measured to an accuracy of 0.25-1.0°C (depending on altitude) using a General Eastern thermoelectric hygrometer. Wet-bulb potential temperature (θ_w) was derived from temperature and humidity measurements by applying formulae from *Bolton* [1980].

3. Flight A315, March 2, 1994

3.1. Synoptic Situation

This case study is based on aircraft measurements over southwest England on March 2, 1994. Surface pressure analysis and positions of fronts reproduced from the European Meteorological Bulletin (Figure 2) illustrate the synoptic situation in the region at the time of the measurements, together with the aircraft track. The dominant feature over the North Atlantic Ocean is the low-pressure system with a central pressure of 965 mbar located southeast of Greenland, and its associated fronts, extending down through the North Sea into northern France and out across the Atlantic. Between 12 and 24 hours prior to measurements a baroclinic wave developed on the cold front over the Atlantic, By the time the measurements were made its apex was located at 47°N, 21°W (Figure 2), while the main frontal system had passed over the United Kingdom.

3.2. Radiosonde Observations

From its surface position extending eastward from the wave apex, the warm front section of the wave sloped northward as the frontal surface rose through the troposphere. Several radiosonde ascents intersected the frontal surface: that from Camborne (50.2°N, 5.3°W) at 1100 UT showed a stable layer and a sharp change in humidity between 4.0 and 4.8 km (Figure 3a); while the 1200 UT ascent from Brest (48.5°N, 4.4°W) showed a

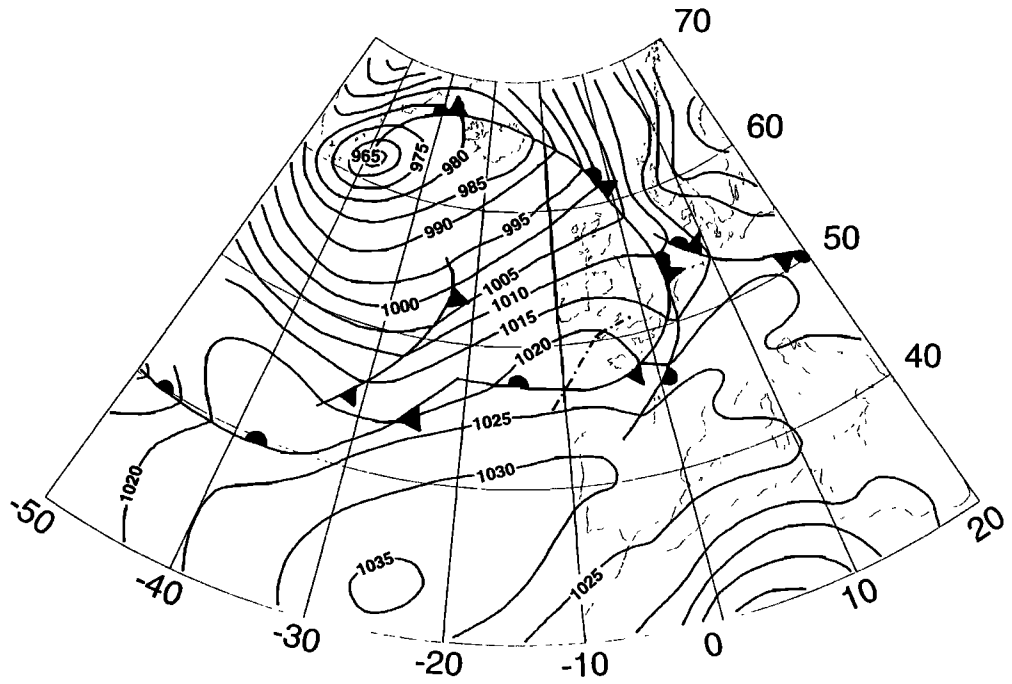

Figure 2. Surface pressure analysis for 1200 UT, March 2, 1994 (based on the European Meteorological Bulletin). The aircraft's track is shown as the thick dash-dotted line.

similar feature between 2.5 and 3.0 km (Figure 3b). This translates into a frontal slope of 120:1 which lies within the range of warm frontal slopes found by *Freeman* [1961]: 110:1 to 200:1. The Camborne ascent exhibits extremely dry air above the front, while the Brest ascents exhibits a layer of dry air immediately above the front, a layer of moist air (greater than 70% relative humidity) above that, and a layer of very dry air at a similar altitude to Camborne. Dry air is an indicator of subsidence, so we can say in this case that air in the midtroposphere above the frontal surface had recently descended from higher levels rather than being lifted from the boundary layer.

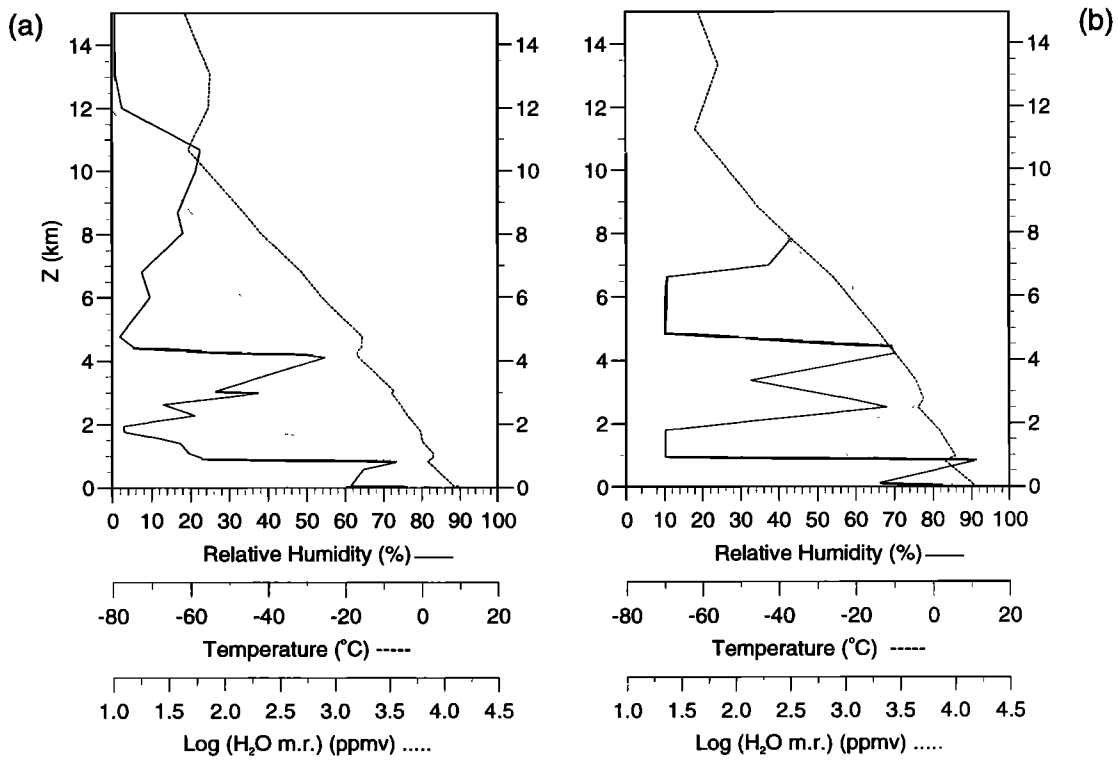

Figure 3. Radiosonde ascents from (a) Camborne at 1100 UT, March 2, 1994; and (b) Brest at 1200 UT, March 2, 1994. Dashed line, temperature; solid line: relative humidity, dotted line: mixing ratio.

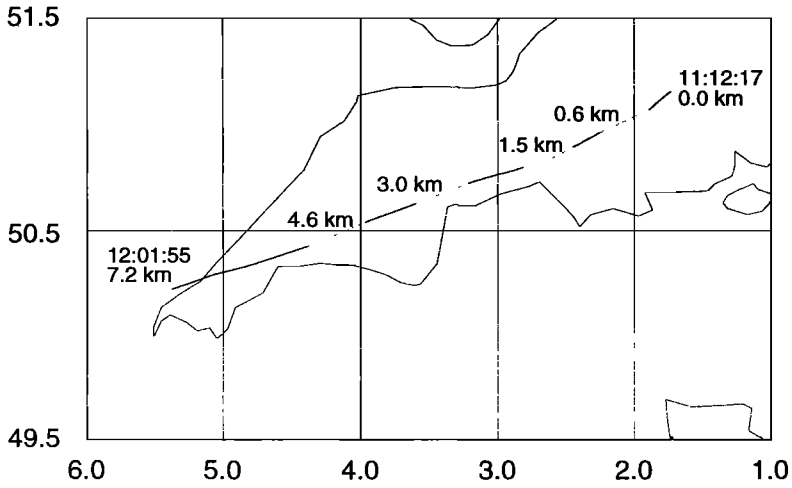

Figure 4. The path of the aircraft over southwest England during the collection of the measurements presented in Figure 5. The map covers the region 49.5°-51.5°N, 1.0°-6.0°W. Dotted sections indicate horizontal runs at the altitudes noted; solid sections indicate ascent of the aircraft.

3.3. Aircraft Observations

Measurements presented in this case study were taken during the execution of a stepped profile by the aircraft over southwest England (Figure 4). The profile commenced at 1112 and ended at 1202 very near to Camborne. Comparison of Figure 4 with Figure 2 reveals that the aircraft sampled air northward of the surface position of the warm front.

Profiles of ozone, temperature, relative humidity (with respect to water), water vapor mixing ratio, NO_y, CO, and θ_w are shown in Figure 5 and, as expected, the temperature and humidity profiles are very similar to those measured by the Camborne radiosonde. The aircraft commenced its ascent in the colder air below the front, intersected the frontal surface at between 4.4 and 4.8 km, and continued to ascend in the warm air above and equatorward of the front. Therefore, in Figure 5, measurements below 4.4 km represent air north of the front; and those above 4.8 km represent air south of the front. Note that the aircraft shows a shallower frontal zone than the radiosonde because of the horizontal component of its motion.

It is immediately evident from Figure 5 that θ_w is the most appropriate parameter for identifying different air masses in the profile; its value is reasonably uniform within an air mass, and air mass boundaries are clearly identified by sharp gradients in θ_w at 0.7, 2.7-3.1 km, 4.4-4.8 km, and 5.8-6.1 km. These boundaries are also characterized by enhanced static stability that acts to inhibit mixing by convection. A much more gradual increase in θ_w occurs between 1.0 and 2.7 km within a very dry air mass; this feature and the low relative humidity values are both characteristics of air which has subsided [*Wickham*, 1970]. The chemical composition of the five air masses evident in the profile will now be discussed briefly, starting with the lowest air mass.

The well-mixed boundary layer below 700 m has a uniform water vapor and ozone mixing ratio, but CO and NO_y concentrations increase with height to 400 and 15.2 ppbv, respectively. These values are much higher than those in the free troposphere and are consistent with the boundary layer sources of these two species. The subsided air (0.8-2.7 km) has no uniform chemical or thermodynamic signature. A small temperature inversion just below 1.7 km separates the relatively ozone-rich layer (36 ppbv) of uniform θ_w directly above the boundary layer from lower ozone values farther up. NO_y and CO are variable, so the layer 0.8-2.7 km is best considered as an interleaving of air from many different sources. Note that much of the thermodynamic data (temperature, dew point) were missing between 1.7 and 2.7 km; there was none between 1.7 and 2.1 km and a number of data gaps thereafter, identifiable by straight lines in the mixing ratio profile. Thus the apparent steady increase in θ_w in this part of the profile in Figure 5 is illusory.

The transition from this subsided air mass to the one immediately above it (i.e., that between 3.1 and 4.4 km altitude) is not only marked by a sharp increase in θ_w and a shallow layer of stable air, but also by an increase in ozone (from 36 to 44 ppbv) and a decrease in both CO (195 to 160 ppbv) and NO_y (700 to 500 pptv). This is clearly a case where chemical tracers (especially CO and ozone) identify an air mass boundary as effectively as a thermodynamic tracer. The air mass between 3.1 and 4.4 km lies immediately below the frontal surface and, like the two air masses below it, resides on its cold side. The remarkably uniform concentrations of ozone, CO, water vapor and NO_y in this air mass indicate that considerable mixing has occurred within it.

The remarkable feature about the air mass residing immediately above the front (i.e., between 4.8 and 5.8 km) is its low humidity: between 5 and 10%. This feature captured by the aircraft's instrumentation is confirmed by the Camborne radiosonde ascent (Figure 3a). Once above the frontal zone, ozone decreases from 42 to 32 ppbv. CO

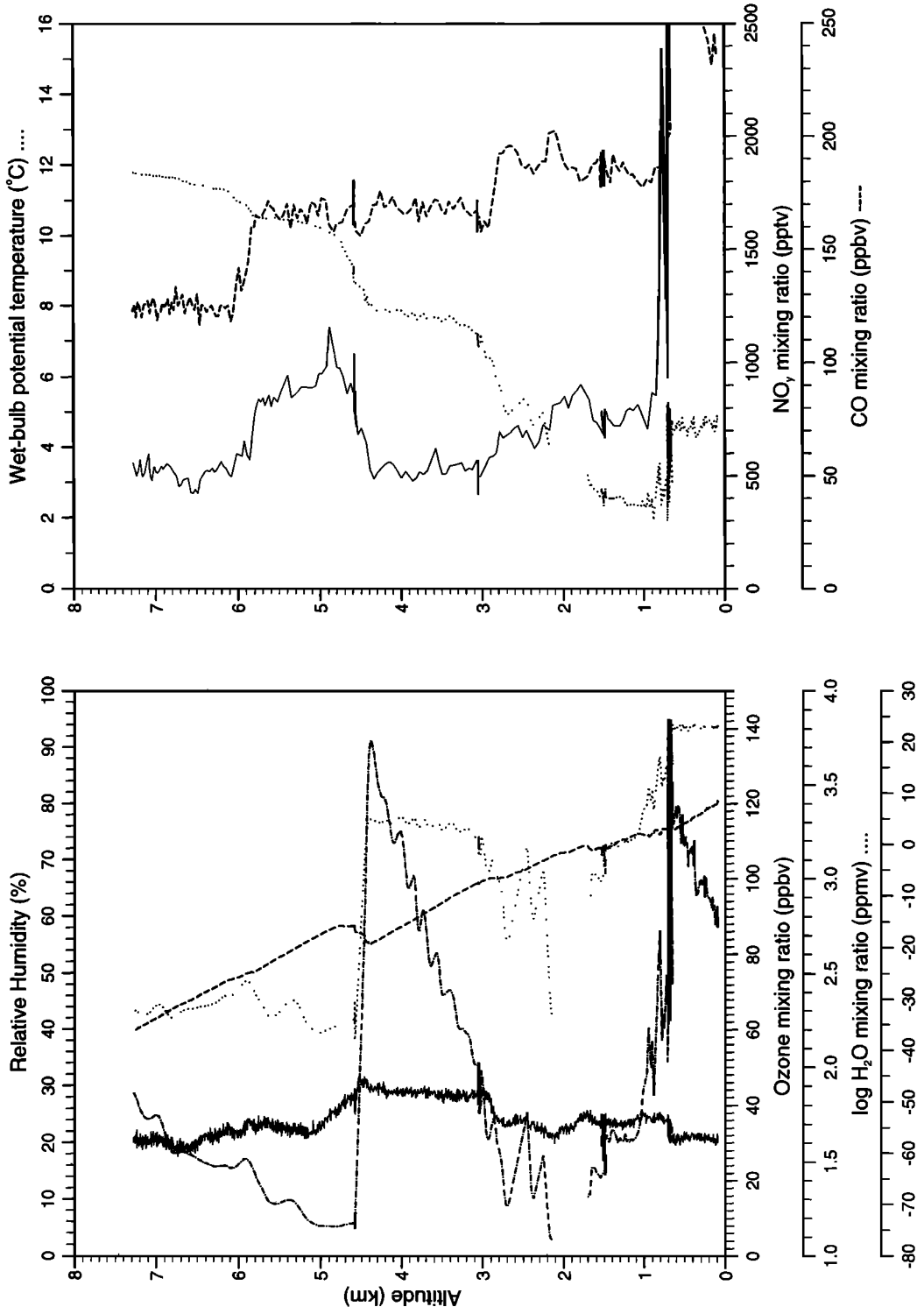

Figure 5. Profiles of ozone (solid), temperature (dashed), relative humidity (dash-dotted), and water vapor mixing ratio (dotted) on the left-hand graph, along with NO_y (solid), CO (dashed), and θ_w (dotted) on the right hand graph. The location of the measurements is indicated in Figure 4. Air mass boundaries can be clearly seen in the θ_w profile at 0.7, 2.7-3.1 km, 4.4-4.8, and 5.8-6.1 km. Maximum concentrations of 400 and 15.2 ppbv were measured for CO and NO_y, respectively in the boundary layer (700 m altitude).

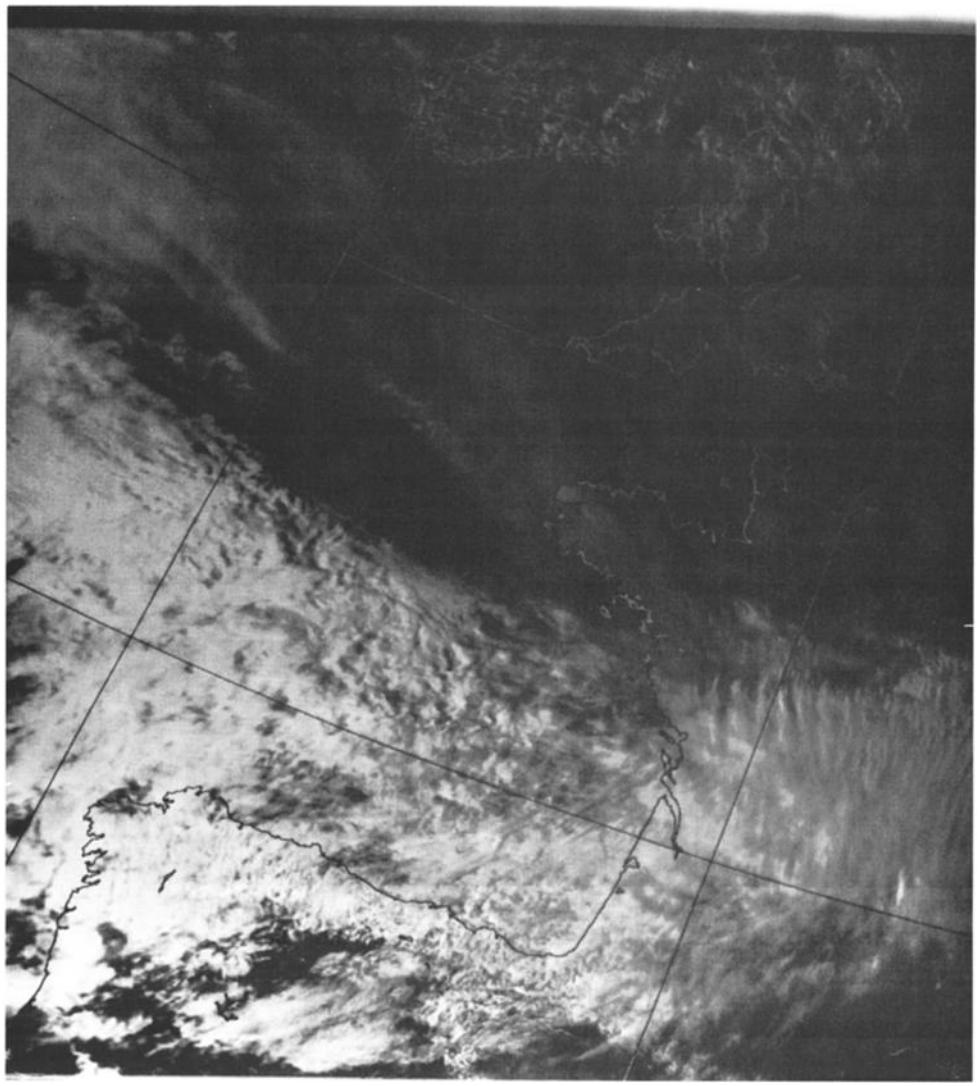

Figure 6. Visible NOAA satellite image captured at 1540, March 2, 1994.

is fairly uniform within this air mass, whereas a slight decrease with altitude is seen in NO_y (from 950 to 850 pptv) and NO (from 40 pptv to below 20 pptv, not shown). CO concentrations are almost identical to those below the frontal surface; however, the substantially different humidity and θ_w values clearly indicate that these are indeed separate air masses of different origins. Unlike the air mass transitions at 2.7-3.1 km and 5.8-6.1 km, this is a case where CO is not as successful as θ_w at identifying an air mass boundary, which makes the point that one tracer alone is not sufficient to delineate all air mass boundaries. A sharp drop in CO and NO_y and an increase in θ_w of ~1°C then mark the transition to the uppermost air mass.

3.4. Satellite Images

Visible and infrared satellite images captured by the NOAA 11 satellite at 1540 on March 2, 1994 (i.e., between 2 and 4 hours after the time that measurements were made) can be seen in Figures 6 and 7. Comparison with Figures 2 and 4 reveals that the aircraft measurements in Figure 5 were made in cloud-free air. Note that the cloud feature to the west of Cornwall has a well-defined convex edge on its cold side in both the visible and infrared images; this is a characteristic associated with waves on a cold front [*Kurz*, 1995] and represents the rising motion within a warm conveyor belt (WCB) associated with the developing wave where the flow (as indicated by the cloud cover) is anticyclonic and on the cold side of the surface front. The small amount of cloud cover indicates that this WCB is much less well developed than that associated with a mature low-pressure system, such as is visible to the south of it. Therefore Figure 5 represents the crossing of a front with no cloud in the immediate vicinity, thus indicating that this frontal surface is a passive air mass boundary rather than an active region of ascent.

3.5. Trajectory Analysis

Five-day three-dimensional back trajectories were run on archived data from the U.K. Meteorological Office's local area model (LAM). The horizontal resolution of the

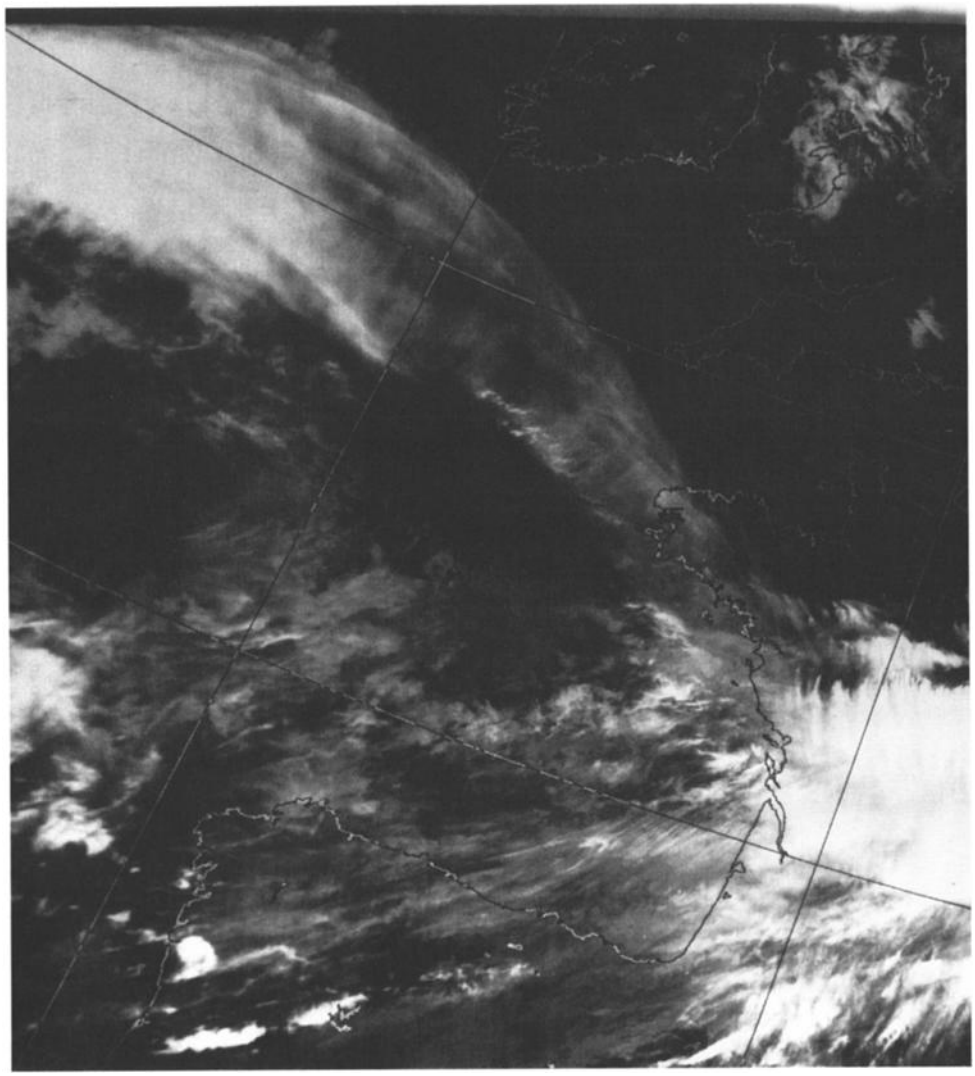

Figure 7. Infrared NOAA satellite image captured at 1540, March 2, 1994.

data was 0.442° (approximately 50 km). Horizontal wind velocities were available on the following eight pressure levels in the troposphere: 950, 850, 700, 600, 500, 400, 300, and 250 mbar, while vertical velocities were only available at 850, 700, 500, and 250 mbar. Output was available every 3 hours, and fields were linearly interpolated for intermediate times. A variable timestep was used in the calculations, depending on the curvature of the wind fields; in all cases the time step was less than 15 min. Back trajectories were run from various pressure levels between 800 and 400 mbar at 50.6°N, 4.0°W, the location where the aircraft crossed the front, and from four points half a degree away from this point. Once they descended below 850 mbar (approximately 1.5 km), they were not continued back since no vertical wind data were available below this level. If the trajectories reached the perimeter of the LAM (its corners are at 45°N, 117°W; 46°N, 77°E; 11°N, 62°W; and 12°N, 21°E), they were continued back using global model analyses; these were available every 6 hours with a horizontal resolution of 1.875° by 1.5°.

Back trajectories from the location where the aircraft crossed the front are shown in Plates 1a and 1b; they represent the history of air terminating above and below the front, respectively, and are representative of the clusters of trajectories generated. The positions of each trajectory relative to the surface fronts during the 36 hours prior to the time of measurements are shown in Plate 2; colors and symbols match with those in Plate 1. It can be seen that all the trajectories originated behind the surface polar front over the western Atlantic and they all remained poleward of it during their history. If their vertical displacement, as shown in Plate 1, is considered, the trajectories divide into three distinct families: (1) those that end between 5.0 and 7.2 km (solid circles); (2) those that end between 3.9 and 4.6 km (red, green, and navy open circles); and (3) those that end between 2.0 and 3.1 km (light blue, pink, and yellow open circles).

The uppermost family of trajectories (solid circles) were located in the upper troposphere (between 7 and 8 km) over the Great Lakes region of North America 48 hours prior to measurements. At this time, they were well

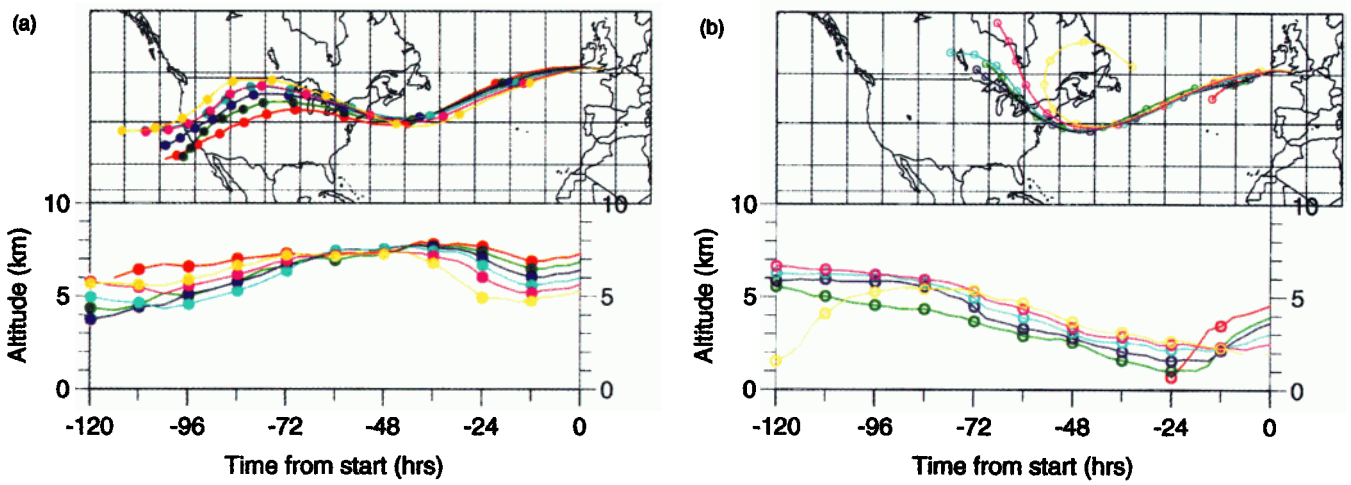

Plate 1. Five day back trajectories from 50.6°N, 4.0°W indicating the history of the air sampled by the aircraft in Figure 5. Circles indicate the trajectory positions at 12 hourly intervals for (a) trajectories terminating above and (b) those terminating below the frontal surface. The red open circle trajectory was terminated after 24 hours because it descended below 850 mbar (limit of available vertical wind data).

behind the polar front. During the next 36 hours this air subsided (Plate 1a) such that 12 hours prior to measurements it was located to the north of the wave apex (Plate 2c). The behavior of this air mass is clearly not related to the development of the baroclinic wave. The air simply traveled around the base of an upperair trough (apparent on the 500 mbar chart over the western Atlantic) during the final 48 hours and fed into the region above the front. Individual clusters within this family of trajectories stayed together; 120 hours earlier they were dispersed by less than 750 km from the location of the central point in Plate 1a. There is a systematic variation with the height of the clusters, with the upper trajectories (navy, red, and green) originating farther south.

This is consistent with the trace gas measurements, which indicate that two different air masses are present

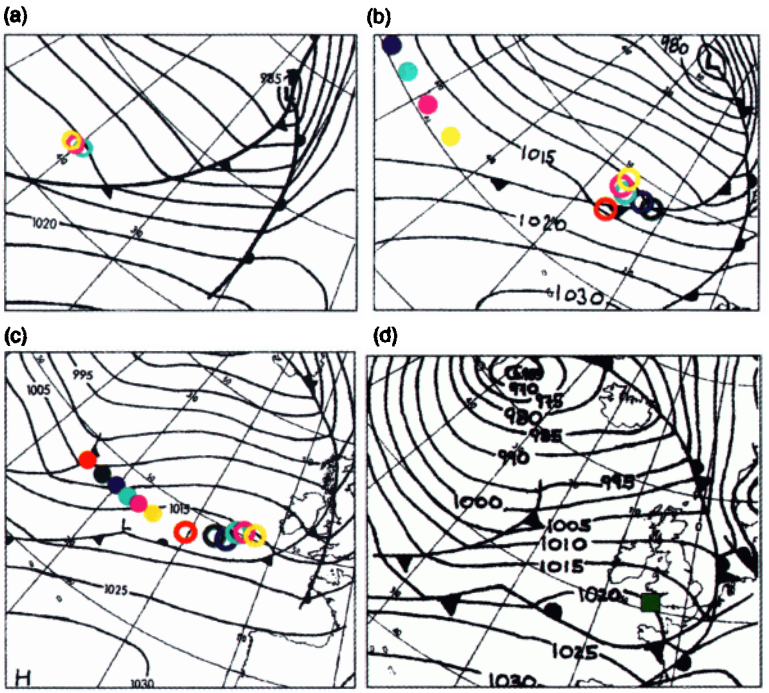

Plate 2. The positions of the trajectories plotted in Plate 1 relative to the developing baroclinic wave at (a) 36 hours prior to measurements (0000 UT, March 1, 1994), (b) 24 hours prior to measurements (1200 UT, March 1, 1994), (c) 12 hours prior to measurements (0000 UT, March 2, 1994), and (d) at the time of the measurements; that is, the location of the measurements is marked by a green square. Note that as in Plate 1, open circles represent trajectories that terminate below the frontal surface, while solid circles represent those terminating above the frontal surface. Colors match with those in Plate 1.

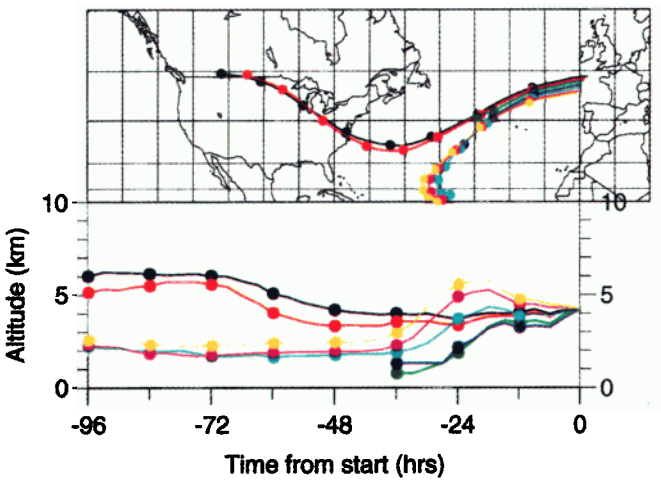

Plate 3. Trajectories indicating the four-day history of air whose characteristics are plotted in Figure 8. Dots indicate the trajectory locations at 12 hourly intervals. The lower two trajectories (navy and green) were terminated when they descended below 850 mbar, as in Plate 1.

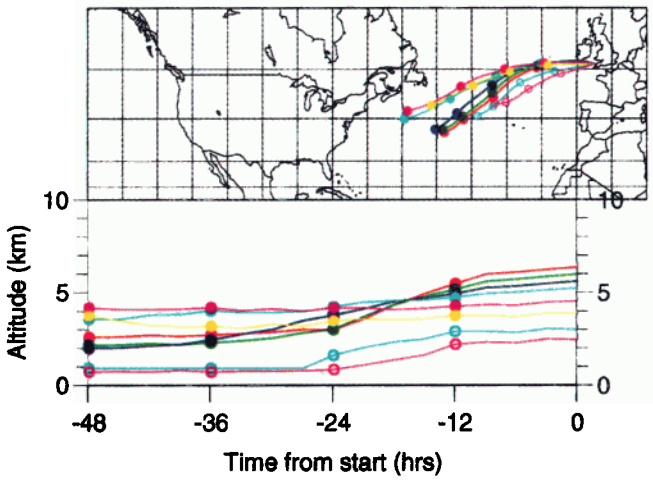

Plate 4. Forty-eight-hour back trajectories from 51.1°N, 5.0°W indicating the history of the air sampled by the aircraft in Figure 13. Circles indicate the trajectory locations at 12 hourly intervals.

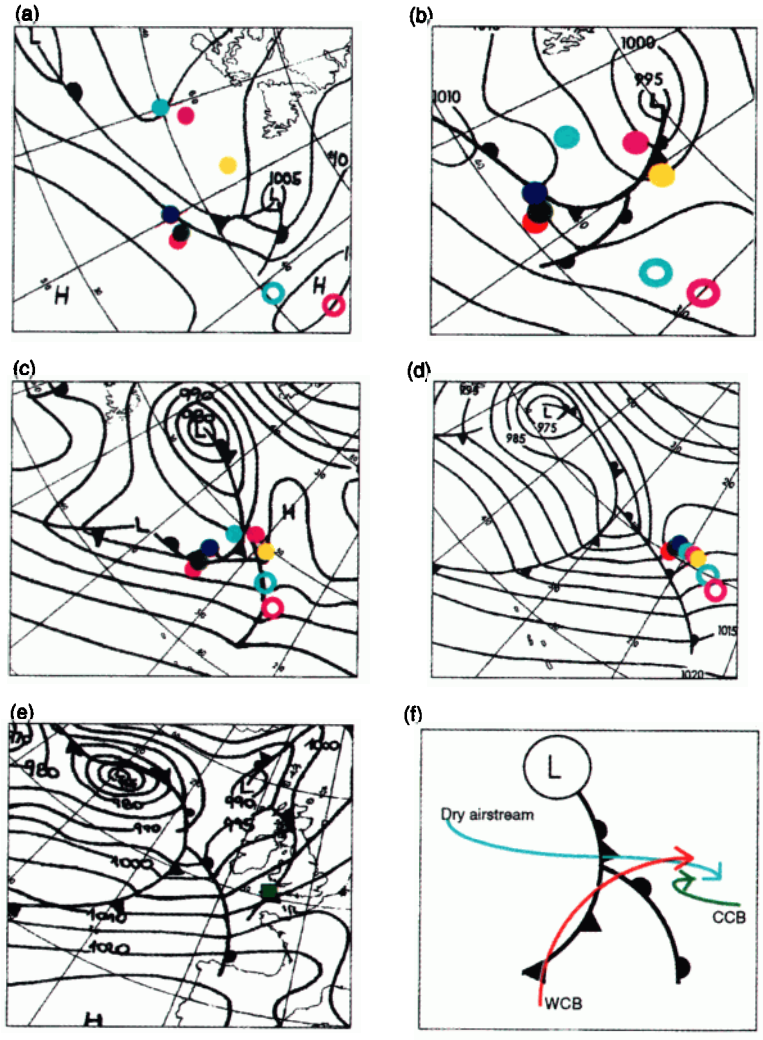

Plate 5. The positions of the trajectories plotted in Plate 4 relative to the low-pressure system at (a) 48 hours prior to measurements (1200 UT, April 23, 1994), (b) 36 hours prior to measurements (0000 UT, April 24, 1994), (c) 24 hours prior to measurements (1200 UT, April 24, 1994), (d) 12 hours prior to measurements (0000 UT, April 25, 1994), and (e) the time of measurements (1200 UT, April 25, 1994). The green square in Plate 5e indicates the location of the measurements, where the trajectories terminate. Colors and symbols match with those in Plate 4 with open circles denoting the lowest two trajectories. Plate 5f indicates the flow of the major airstreams identified relative to the system.

above the front, identified by their significantly different CO, NO_y and θ_w values. On February 25, 1994, 120 hours prior to the measurements, a depression was located over the eastern Pacific. The more northerly trajectories (light blue, pink, and yellow solid circles) originated behind its surface cold front while the others (navy, green, and red solid circles) originated in the warm sector. Two of these southerly trajectories (navy and green solid circles) also ascended considerably (~2.5 km) during the first 60 hours of the sequence shown in Plate 1a. This rising motion within the warm sector suggests that these trajectories represent air that ascended as part of the WCB of the low-pressure system. The gradient in CO and NO_y at 6 km therefore represents a latitudinal difference in origin with the cleaner air of subtropical origin contrasting with the higher CO and NO_y content of higher-latitude air (this point becomes clearer when Figure 8 is considered in the next section. The subsequent ascent and descent of these air masses, indicated by the trajectories, accounts for their low relative humidity.

Consider the trajectories ending between 2.0 and 3.1 km (light blue, pink, and yellow open circles in Plate 1b), that is, within the dry air mass some distance below the front in Figure 5. As expected, the trajectories indicate that this air has recently subsided. The lifting condensation level for air at, for example, 2.5 km is approximately 6 km, and indeed two of these three trajectories (light blue and pink) have descended from 5-6 km in the 4 days prior to the measurements, thus explaining the low humidity values observed. The air between 2 and 3 km displays the highest CO concentrations seen in the free troposphere in Figure 5. Unfortunately, the trajectory clusters for this group showed substantial dispersion; the end points were scattered over eastern Canada and the northeast United States, so no precise conclusion about the origin of this air mass can be drawn.

The trajectories terminating between 3.5 and 4.6 km (red, green, and navy open circles) all indicate rapid ascent from below 2 km during the 24 hours prior to the measurements (Plate 1b). These clusters showed less dispersion than those in the dry air mass, with most of the end points near the Great Lakes region in the mid-troposphere 5 days previously, within 500 km of the locations of the central points in Plate b. Some of the trajectories in the green and navy clusters, and all those in the red cluster, descended too far to be continued back beyond 24 hours. These trajectories terminated in the comparatively ozone-rich air mass resident immediately below the frontal surface (Figure 5). They rose from low level close to the location of the low-pressure center developing on the front (red, green, and navy open circles in Plates 2b and 2c), after descending from the midtroposphere in the previous 4 days. Support for a midtropospheric, rather than a boundary layer source for this air is provided by the low humidity, which is not consistent with uplift from the boundary layer. The NO_y content of this air mass is also low, consistent with a midtropospheric source.

3.6. Sampling of Warm Conveyor Belts

Following execution of the stepped profile shown in Figure 5, the aircraft descended to an altitude of 4.3 km then continued in level flight on a heading of 255°. Inspection of the descent profile (not shown) indicates that the aircraft did not reenter the frontal zone; that is, it remained on the warm side of the front.

A comparison of satellite images taken at 0847 UT (not shown) and 1540 UT (Figures 6 and 7) on the day in question reveals that during this horizontal run the aircraft was initially located in clear air. It then entered the region occupied by the convex cloud feature associated with the WCB of the developing wave. Finally, it sampled the region occupied by the WCB of the mature low-pressure system, which extended westward over the Bay of Biscay (Figure 6). Measurements from this run (along with those gathered during the previous profile and subsequent descent) are shown in Figure 8. Inspection of the ozone trace reveals that three different air masses were sampled during the horizontal run: between the start of the run and 45,600 s (1240 UT); between 45,600 s and 46,700 s (1258 UT); and from 46,700 s onward. These three segments correspond on the satellite image with clear air conditions, the wave WCB, and the mature WCB, respectively.

The supposition that three different air masses were sampled is further confirmed by back trajectories calculated from the aircraft's position during its progress southward (Plate 3). The two trajectories (black and red) terminating near the start of the run traveled across from the midtroposphere above North America. A similar history was assigned to the air sampled above the front in Figure 5. Indeed, the humidity, CO, and NO_y values sampled immediately above the front (4.8 to 5.8 km in Figure 5 and 42,200-42800 s in Figure 8) and during 44,600-45600 s are sufficiently similar to suggest that the aircraft sampled the same air mass in these two periods, that is, dry air that traveled from North America on the warm side of the front.

The second segment of the horizontal run (45,600-46,700 s) displays the highest ozone concentrations of the time series, up to 50 ppbv. NO_y and CO concentrations are similar on average to the first segment, although they are more variable. This air rose from the boundary layer during the previous 36 hours, as shown by the green and navy trajectories in Plate 3. The ascent of this air, along with its location (near to the convex cloud feature in Figures 6 and 7), leads to the conclusion that it is part of the WCB associated with the developing wave. The characteristics of this WCB are therefore enhanced ozone (40-50 ppbv), variable relative humidity (20-70%), CO in the range 150-180 ppbv, and variable NO_y (650-950 pptv).

During the final segment of this horizontal run, the aircraft flew within the thick cloud band associated with the mature WCB. The low-latitude, low-altitude origin of the three trajectories terminating within this segment (yellow, pink, and light blue trajectories, Plate 3),

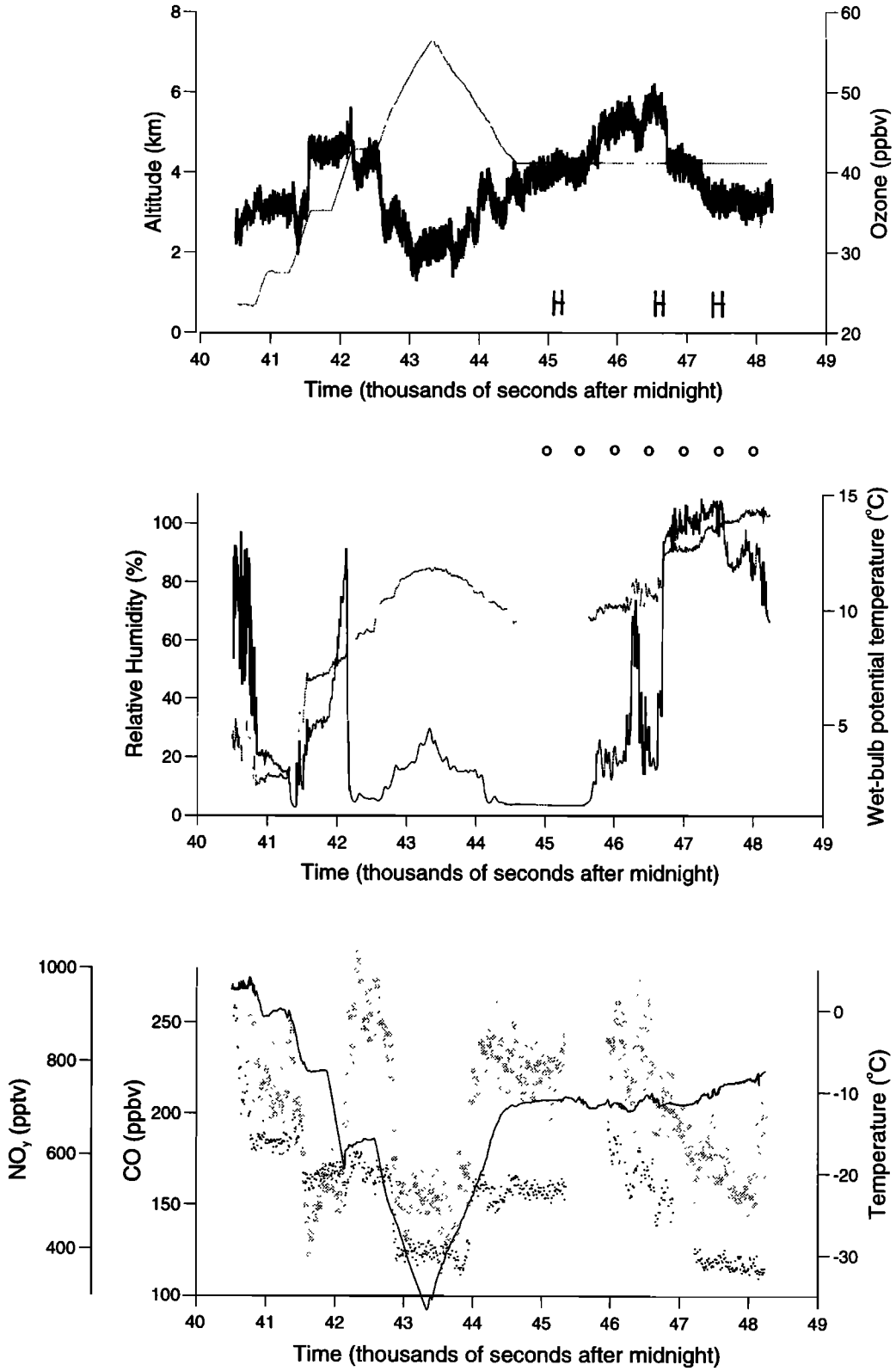

Figure 8. (top) Measurements of ozone (thick line) and altitude (thin line); (middle) measurements of relative humidity (lower line) and θ_w (upper line); (bottom) measurements of temperature (solid line), CO (dark dots), and NO_y (light circles), during the aircraft's progress southward. (Note that a calibration of these last two instruments results in a data gap between 45,400 and 46,000 s.) Air mass boundaries are clearly seen at 45,600 s (1240 UT) and 46,700 s (1258 UT). Times during which bottle samples were taken are shown by H symbols on the top graph. Times corresponding to the starting locations of the trajectories in Plate 3 are denoted by open circles below the top graph; reading from left to right they correspond to the black, red, green, navy, blue, pink, and yellow trajectories.

together with their motion relative to the low-pressure system and its associated fronts, are consistent with the notion that measurements taken after 46,700 s in Figure 8 represent sampling of a mature WCB. Two distinct air masses occur within this WCB, the first between 46,700 and 4,7250 s, with θ_w ~ 12.5°C, ozone ~ 41 ppbv, CO ~ 155 ppbv, and NO_y ~ 600-700 pptv; and the second after 47,300 s with θ_w ~ 14°C, ozone ~ 36 ppbv, CO ~120 ppbv, and NO_y ~ 500-600 pptv. Note that ozone is (anti) correlated more closely with θ_w than either of the other two species, perhaps because of the photochemical sink for ozone in the subtropical marine boundary layer.

Bottle samples were obtained during each of the three segments of this run and were subsequently analyzed via a gas chromatograph for halocarbon and hydrocarbon concentrations [*McKenna et al.*, 1995]. The results are shown in Table 1. There is a clear division between the three bottles: the first had the highest concentrations of alkanes, while the third contained less of every compound. Taken together with the CO, NO, and NO_y (Table 2), these measurements are consistent with a midlatitude source for the first two bottle samples and a subtropical source for the third. Note that the CO and NO_y from 47,300 s on in Figure 8 match measurements between 42,900 and 43,900 s, in the air mass previously deduced to have originated in the subtropical Pacific. The ozone difference between these two segments is also consistent with the lower ozone concentrations measured over the subtropical Pacific than the Atlantic (compare *Weller et al.* [1996] with *Browell et al.* [1996]). The two midlatitude bottles are significantly different; the larger concentrations of alkanes in the first bottle suggest a more recent component of polluted continental air, which is reinforced by the greater difference for the heavier (more reactive) alkanes and the detectable NO corresponding to the first bottle. The CO and NO_y corresponding to the two bottles are very similar,

Table 1. Concentrations Derived From Bottle Samples Collected During the Horizontal Run at 4.3 km on Flight 1 (A315)

	Time of Sample, s After Midnight		
	45,097-45,215	46,550-46,680	47,390-47,535
Position	48.7°N, 8.0°W (dry air mass)	47.2°N, 9.7°W (wave WCB)	46.4°N, 10.6°W (main WCB)
N_2O, ppbv	313.9 ± 0.9	321.3 ± 0.9	312.7 ± 0.9
F11, pptv	273.5 ± 0.5	282.3 ± 0.5	274.9 ± 0.5
F12, pptv	529.4 ± 0.2	538.2 ± 0.2	529.3 ± 0.2
Ethane, pptv	2,361 ± 4	2,350 ± 4	1,438 ± 4
Propane, pptv	385 ± 4	321 ± 4	191 ± 4
n-butane, pptv	149 ± 5	75 ± 5	39 ± 5
i-butane, pptv	74 ± 3	47 ± 3	29 ± 3
n-pentane, pptv	52 ± 4	15 ± 4	7 ± 4
i-pentane, pptv	27 ± 3	12 ± 3	6 ± 3
Acetylene, pptv	259.5 ± 1.5	286.5 ± 1.5	122.0 ± 1.5

Values given are the mean and standard deviation of four chromatograms from each bottle.

Table 2. Mean Concentrations of CO, NO, and NO_y During the Periods When the Bottles in Table 1 Were Filled

	Time of Sample, s After Midnight		
	45,097-45,215	46,550-46,680	47,390-47,535
Position	48.7°N, 8.0°W (dry air mass)	47.2°N, 9.7°W (wave WCB)	46.4°N, 10.6°W (main WCB)
CO, ppbv	158 ± 3	156 ± 11	119 ±3
NO, pptv	19 ±10	9 ± 12	9 ± 10
NO_y, pptv	710 ± 14	660 ± 60	570 ± 15

although NO_y was more variable around the time the second bottle was filled (which was at the edge of the second segment). The enhanced acetylene concentration in the second bottle is evidence of anthropogenic pollution, although not as recent as in the first bottle.

To summarize, Figures 8 and Plate 3 reveal that ozone-rich air rose out of the boundary layer on the warm side of the front during the development of a baroclinic wave. They also illustrate the contrasting signatures of the two WCBs, one of a midlatitude origin and the other of a subtropical oceanic origin. Given the high concentration of N_2O, F11, F12, and CO in the wave WCB, a stratospheric source for the elevated ozone is unlikely, so we conclude that it was of photochemical origin. Finally, the most significant chemical transition shown in Figure 8 occurs at 46,700 s, when, despite a substantial change in humidity resulting in a change in θ_w, no significant change in temperature occurs. The significant temperature discontinuity occurred farther north, during the profile shown in Figure 5. This is therefore a clear indication that chemical fronts and temperature fronts are not always colocated and confirms that θ_w is a more appropriate meteorological indicator of air mass boundaries than is temperature.

4. Flight A325, April 25, 1994

In an interesting contrast to A315, a second case study is presented here of measurements through the warm front of a mature occluded system.

4.1. Synoptic Situation

An aircraft profile was measured around midday on April 25, 1994, off the Cornish coast (Figure 9). At this time a cold front lay approximately north-south over the United Kingdom in the European Weather Bulletin analysis but was absent in the corresponding U.K. Meteorological Office analysis (not shown). The satellite cloud images (Figures 11 and 12) show that this weak feature lay well to the east of the aircraft profile. The main frontal system influencing the region of the measurements was associated with a low of 965 mbar centered at 55°N, 30°W. Its warm front was approaching the United Kingdom from the southwest with warm

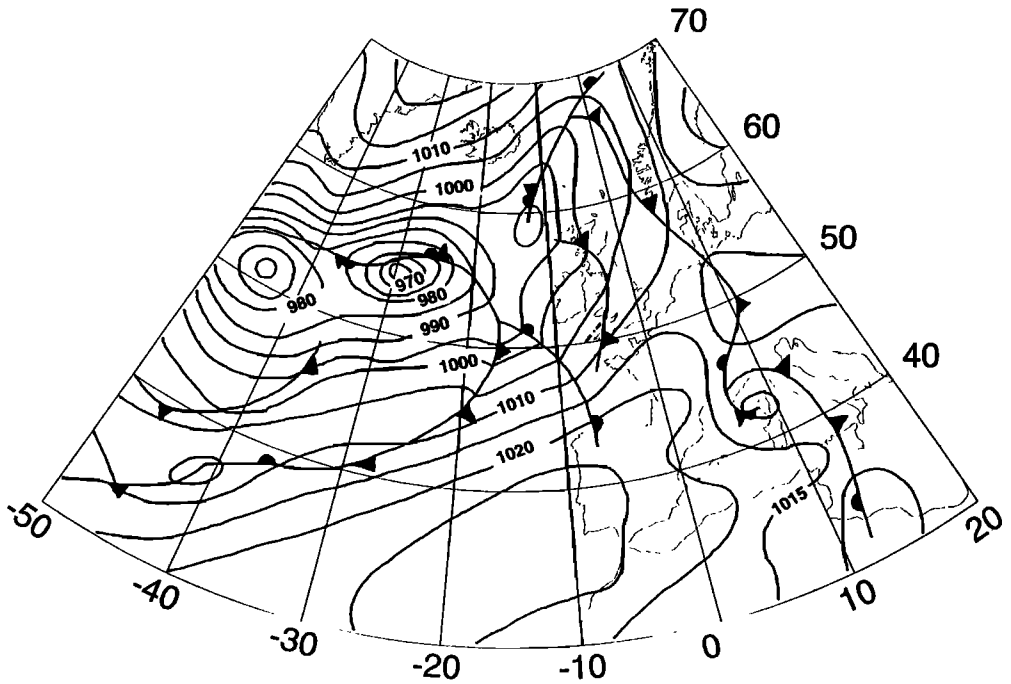

Figure 9. Surface pressure analysis for 1200 UT, April 25, 1994 (based on the European Meteorological Bulletin). The aircraft's track is shown as the thick dash-dotted line.

southerly air being advected behind it. During the previous 48 hours this system tracked across the Atlantic from a location east of Newfoundland, deepening from a central pressure of 1005 mbar at 1200 UT, April 23, 1994, to 965 mbar at the time of the flight, 48 hours later. The system occluded during the first 12 hours. A high-pressure system also developed and tracked across, south of the warm front, toward Spain. As in the first case study, the polar front is visible trailing out across the Atlantic, acting as a site for further cyclogenesis.

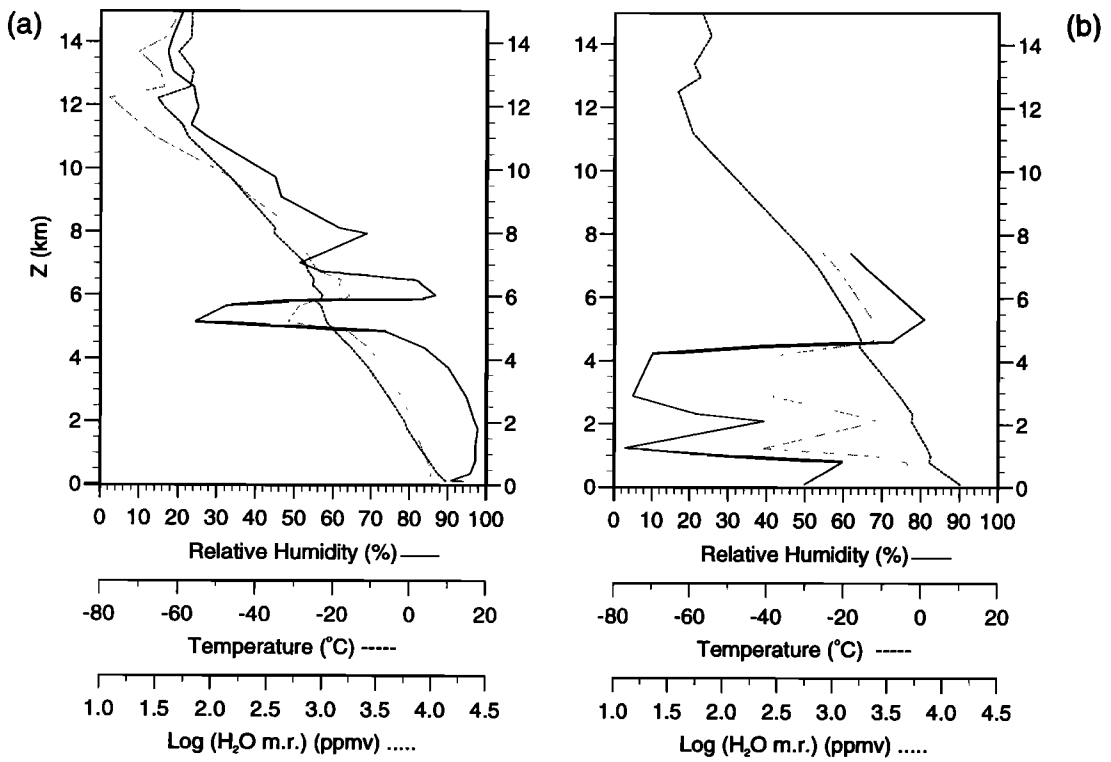

Figure 10. Radiosonde profiles from (a) Camborne at 1100 UT, April 25, 1994; and (b) Valentia at 1200 UT, April 25, 1994. Dashed line, temperature; solid line, relative humidity; dotted line, mixing ratio.

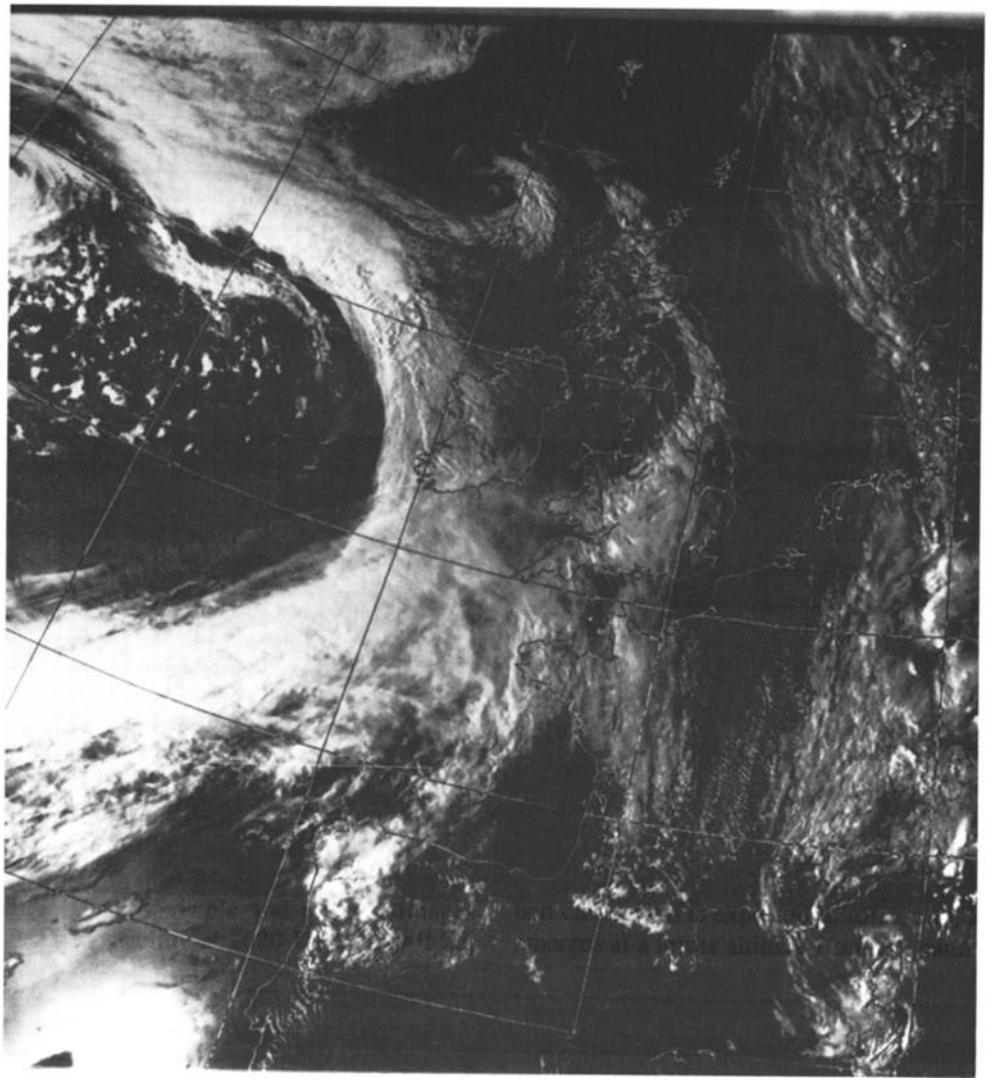

Figure 11. Visible NOAA satellite image captured at 1621, April 25, 1994.

4.2. Radiosonde Observations

From its surface position marked in Figure 9 the warm front sloped northeast as it rose up through the troposphere. Radiosonde ascents from Camborne (50.2°N, 5.3°W, Figure 10a), Bordeaux (44.8°N, 0.7°W), and Santander (43.5°N, 3.8°W) at 1100 UT intersected the frontal zone at altitudes of 5.7, 7.7, and 5.2 km respectively. There was also an ascent from Brest (48.5°N, 4.4°W) at 1200 UT, but its humidity sensor appears to have become saturated thus making identification of the frontal surface difficult. The ascent did, however, display stable air between 5.5 and 6.5 km indicating the probable altitude of the frontal zone. A front is also clearly seen in the ascent from Valentia (51.9°N, 10.3°W, Figure 10b) which is discussed in the next section.

4.3. Satellite Images

Figures 11 and 12 show visible and infrared images from by the NOAA 11 satellite at 1620 UT on April 25, 1994 (approximately 5 hours after the aircraft measurements were made). Both images reveal two cloud bands associated with the frontal system under consideration: a thick, deep band orientated in a southwest-northeast direction parallel to the surface cold front (compare Figure 9); and a lower-level band that emerges from underneath this other band over southern Ireland and extends northwestward toward the low-pressure center. The cloud band parallel to the surface cold front bears all the hallmarks of a warm conveyor belt cloud band, a distinctive feature of which is a sharp western and poleward edge consisting of high cloud [*Browning*, 1990]. As the WCB approached the United Kingdom and Brittany, patterns in both the visible and infrared images indicate that it turns anticyclonically such that over western France the flow in the mid to upper troposphere had a significant northerly component.

The lower-level cloud band located over western Ireland occupies the position where the cold conveyor belt cloud band is expected to form, and, as anticipated, it emerges at a lower altitude from the band associated with

Figure 12. Infrared NOAA satellite image captured at 1621, April 25, 1994.

the WCB: this may be clearly seen on the infrared image. The Valentia radiosonde (Figure 10b) shows the altitude of this cloud band to be about 4.5 km.

4.4. Aircraft Observations

Measurements presented in this case study were taken between 1031 and 1101 UT to the west of Cornwall (Figure 13). The vertical profile presented in Figure 14 commenced at 15 m altitude at 51.1°N, 4.6°W, and ended at 6.7 km at 50.1°N, 6.4°W. In contrast to the previous case study, no horizontal runs were performed during this profile. The aircraft began its ascent on the cold side of the warm front, then passed through the frontal zone, finally sampling the warm air above the front. The latter can be identified in Figure 14 at 5.5 km by the increase in temperature and the large and rapid change in relative humidity and θ_w. Therefore air above 5.5 km in Figure 14 is behind (i.e., equatorward) the frontal surface, while that below 5.5 km is ahead (i.e., poleward) of it.

Consider now the chemical and thermodynamic properties visible in Figure 14. In contrast to Figure 5, the different air masses in Figure 14 cannot be clearly identified as well-defined layers of constant θ_w separated by sharp gradients; the only sharp gradient in θ_w is that associated with the front itself. Starting from the bottom of the profile, there is no inversion present to act as a clear divide between boundary layer and free tropospheric air, and thus the chemicals do not display a sharp transition between boundary layer and higher-altitude concentrations. Up to 3.7 km, NO_y and NO (not shown) decrease gradually with height from 2500 to 600 pptv and 85 to <20 pptv, respectively, while ozone and CO are reasonably constant, at around 41 and 175 ppbv, respectively. At 3.7 km there is a sharp transition to a very dry air mass. Between 3.7 and 4.4 km this air has elevated ozone and NO_y concentrations, and (from 3.7 to 4.0 km) slightly less CO than the air above and below it; these are characteristics suggestive of a stratospheric component. Similar characteristics can be seen in the thin layer between 5.3 and 5.5 km at the top of the dry air mass.

Note that as in the first case study, dry and relatively

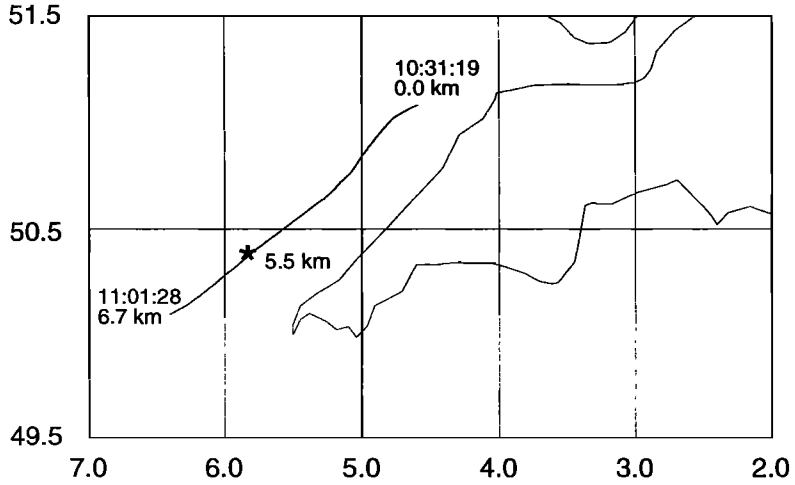

Figure 13. The path of the aircraft during the measurement of the profile presented in Figure 14. The map covers the region 49.5°-51.5°N, 2.0°-7.0°W. The star at 5.5 km identifies the point where the aircraft crossed the front.

ozone-rich air has been sampled below the warm frontal surface. A similar dry air mass was shown by the Camborne radiosonde ascent (Figure 10a), but it was thinner and located at a higher altitude than that in the aircraft profile. This discrepancy is probably due to the sonde being blown northeastward and intercepting the front farther up its slope.

The humidity contrast at the frontal surface itself is remarkable, increasing from less than 10% to over 100% in approximately 150 m; this contributes to a substantial change in θ_w across the front of 5°C. The saturated air immediately above the front (i.e., between 5.65 and 6.0 km) has constant θ_w and contains ozone, NO_y, and CO concentrations similar to the air below the front (i.e., below 5.3 km). A further increase in θ_w at 6.0 km is accompanied by a reduction in the concentration of all three chemicals. Finally, at 6.2 km, a reduction in humidity occurs to give unsaturated air above.

This profile therefore shows the hallmarks of an occluded front, an interleaving of air from diverse locations. It is particular relevant to quote *Carlson*'s [1991, p. 239] description of occlusion as "the result of an evolution of the pattern involving the migration of the cyclone into the cold air, an interleaving of moist and dry air streams...". This interleaving of air streams associated with the occlusion process is illustrated most effectively by the distributions of ozone, CO, and NO_y above and below the front, especially the shallow stratospherically influenced layers at the edges of the dry air mass. Trajectory analysis will now be applied as before to investigate the origins of the main air masses.

4.5. Trajectory Analysis

As with the previous study, three-dimensional back trajectories were calculated from the location of the measurements (50.6°N, 5.5°W) and from four points half a degree away. They were run back from levels between 750 and 425 mbar for just under 5 days (117 hours). The paths of the trajectories ending at 51.1°N, 5.0°W during the final 48 hours are shown in Plate 4. Given that the front was advancing in a northeast direction and that the trajectories were run back from 1200 UT (60 to 90 min after the measurements were made), this position more accurately reflects the position of the aircraft (Figure 13) relative to the front than the other four points. The dispersion of individual clusters was in all cases less than 400 km from the point shown and in most cases was less than 200 km. The trajectories clearly illustrate the interleaving of air from different origins that occurred in the frontal region and may be grouped into three main airflows: (1) upper group, trajectories that end between 5.6 and 6.5 km which began 48 hours previously between 2 and 3.0 km at approximately 37°N, 50°W (red, green, and navy solid circles); (2) middle group, trajectories which end between 3.8 and 5.3 km. These remained at constant altitude during the previous 48 hours and are of a more northerly origin (light blue, pink, and yellow solid circles); and (3) lower group, trajectories which emerge from the boundary layer during the final 24 hours and terminate between 2.5 and 3.1 km (light blue and pink open circles). Trajectories started from the other four points in the clusters revealed the same three groups, but located at different heights, consistent with the slope of the front, the frontal boundary between groups (1) and (2), for instance, occurred around 4.5 km for trajectories starting from 50.1°N, 6°W (150 km southwest of the starting point of the trajectories shown in Plate 4).

The positions of the trajectories in Plate 4 relative to the surface features are indicated in Plates 5a-5e by colored circles. During this 48 hour period the system developed considerably; therefore generating relative wind trajectories would not be meaningful; however, a schematic (Plate 5f) indicates the general motion of the flows relative to the developing system. Interpreting the trajectories in terms of conveyor belt flows, the lower group depicts air that has ascended from below 1 km

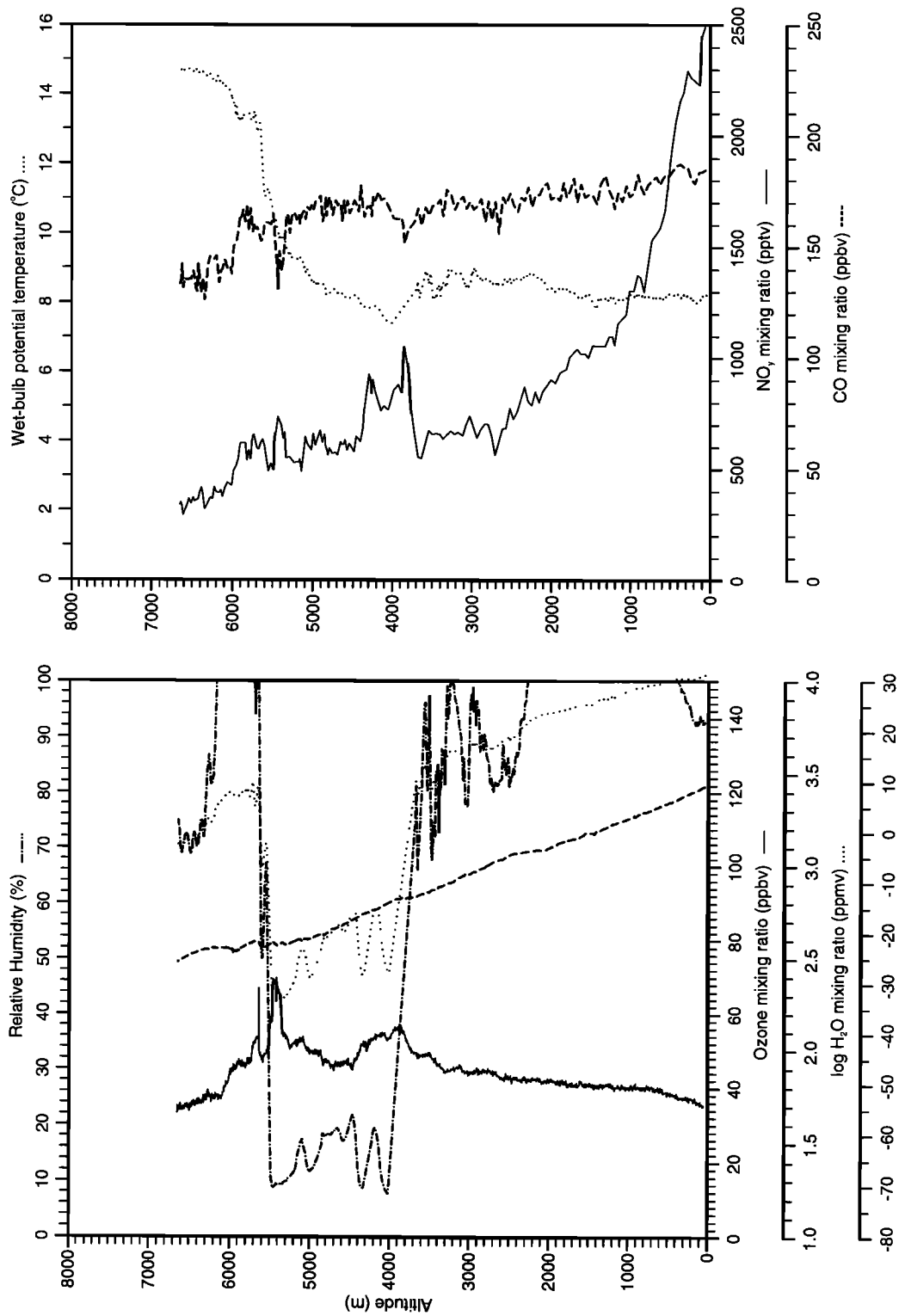

Figure 14. Profiles of ozone (solid), temperature (dashed), relative humidity (dash-dotted), and water vapor mixing ratio (dotted) on the left-hand graph, along with NO_y (solid), CO (dashed), and θ_w (dotted) on the right-hand graph. The location of the measurements is indicated in Figure 13. The warm front can be clearly seen at 5.5 km, and a further air mass boundary at 3.8 km. Thin layers of air with a stratospheric component are present at 3.8 and 5.4 km, embedded in the air mass boundaries.

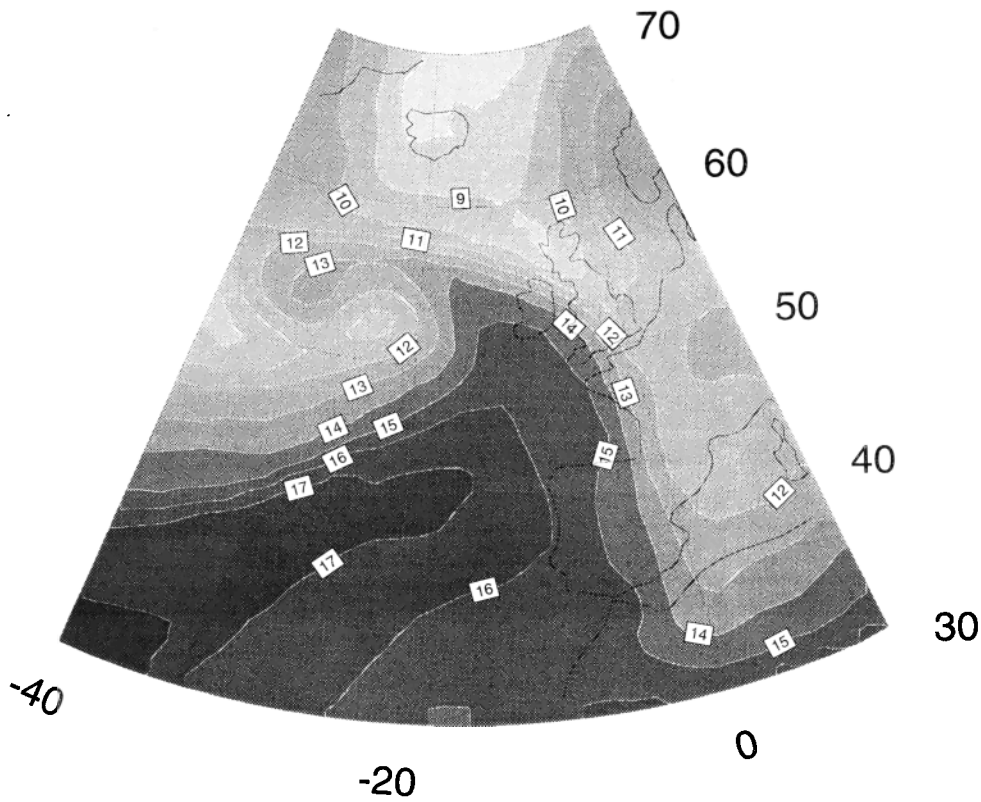

Figure 15. LAM analysis of θ_w values at 500 mbar, valid at 1200 UT, April 25, 1994.

during the previous 24 hours and that has a more southerly track than the other trajectories, indicative of a cold conveyor belt-type flow (although there was little displacement along the front in this case, Plate 5). The upper group depicts saturated, high θ_w flow above the frontal surface; these trajectories clearly trace out the WCB. (The high θ_w air characteristic of the WCB residing within the warm sector can be seen in Figure 15; note, however, that the model considerably underestimates θ_w in the region of the measurements). Forty-eight hours prior to the measurements this group was situated at the base of the free troposphere (Plate 4). During the first 12 hours of the sequence the trajectories remained at constant altitude, advancing toward the position of the surface cold front (Plates 5a and 5b). In the following 12 hours (between 36 and 24 hours prior to the flight), one of the three trajectories (navy) crossed the surface cold front and ascended rapidly, while the other two ascended comparatively slowly (Plate 4).

All three trajectories ascended most rapidly between 24 and 12 hours prior to the measurements, during which time they crossed from the surface cold front, across the warm sector, to a position ahead of the surface warm front, ascending from approximately 3.5 to 5.5 km. During the final 12 hours prior to the flight they ascended slightly (approximately 500 m) and advanced relative to the surface warm front, turning anticyclonically. Clearly, the potential that this well-defined flow has for transporting pollutants (in particular insoluble species) is considerable.

The behavior of the middle group of trajectories is quite different, but it too can be identified with one of the airflows associated with the conveyor belt cyclone model: the dry air stream or intrusion [e.g., *Carlson*, 1980; *Young et al.*, 1987]. Consider the three trajectories that terminate between 3.8 and 5.3 km (yellow, pink, and light blue solid circles). This is air that, 48 hours prior to the flight, resided well to the rear of the cold front (at an altitude of between 3.5 and 4.5 km, Plates 4 and 5a). These trajectories simply advance toward the cold front; however, during the first 12 hours the system occluded, and the trajectory near 3.5 km crossed to the forward side of this newly developed occluded front just slightly north of the triple point. Twelve hours later (Plate 5c), one of the trajectories at 4.5 km (pink solid circle) crossed the occluded front, again near the triple point, before turning anticyclonically in the last 24 hours.

Trajectory history prior to the 48 hours shown indicates that the two trajectories ending at 4.6 and 5.2 km (pink and light blue solid circles) were located north of Alaska (~ 72°N, 140°W) between 6 and 7 km 4½ days prior to the measurements. They subsequently traveled southeastward beneath the anticyclonic side of a jet stream flanking an upper air trough over Labrador. Radiosondes launched from Moosonee (51.3°N, 80.7°W) at 1200 hours on April 22 and Maniwaki (46.4°N, 76.0°W) at 0000 hours on April 23 (near the trajectory positions at those times) showed deep dry, stable layers in the midtroposphere, consistent with a tropopause fold. This is consistent with a stratospheric component to the

air sampled by the aircraft near 5.4 km. The (yellow) trajectory terminating at 4 km also followed a similar path, though at a lower altitude, and there is clear evidence in Figure 14 of a thin, relatively dry, ozone-rich, NO_y-rich and CO-poor layer from 3.7 to 4.0 km, suggesting that it too contains a stratospheric component.

At the time and location of the measurements, the dry intrusion was clearly located underneath the saturated flow of the WCB (Figure 14). This strongly contrasts with the behavior observed in nonoccluded cyclones where the dry intrusion can be seen to penetrate the warm sector (i.e., ahead of the surface cold front) above the WCB thus giving rise to an upper level front [e.g. *Browning and Monk*, 1982; *Browning and Roberts*, 1994]. *Schultz and Mass* [1993] and *Kuo et al.* [1992] both reported a dry intrusion crossing an occluded front; however, neither indicated the height of the WCB in the vicinity of the front. Here the dry intrusion flows below the WCB during the crossing of the occluded front. This is consistent with the many observations of no significant temperature difference across an occluded front in the lower troposphere, with the largest temperature contrast located above the surface [e.g., *Godson*, 1951; *Penner*, 1955; *Galloway*, 1958].

5. Conclusions

Two case studies have been presented of aircraft measurements of trace species near fronts located over the eastern North Atlantic during spring 1994. They were conducted in order to determine whether frontal circulations can transport significant quantities of trace species from the boundary layer to the free troposphere and whether conveyor belts display well-defined chemical signatures. During the first case study (flight A315), in answer to the first point, it has been demonstrated that air (and ozone) was lifted from the boundary layer into the free troposphere by a warm conveyor belt during the development of a baroclinic wave on the polar front over the eastern Atlantic (second segment in Figure 8). This air displayed higher ozone concentrations than elsewhere within the sampled profile, so in this case the upward motion associated with baroclinic wave development contributed positively to the ozone content of the free troposphere.

In addressing the second point it has been clearly demonstrated that conveyor belts do exhibit well-defined chemical signatures but that a number of chemical species must be measured to delineate air mass differences unambiguously. For instance, dry, ozone-rich air is not in itself evidence of a stratospheric origin, as shown clearly in Figure 14 where the low CO which is characteristic of such air is only found in narrow layers within a dry, relatively ozone-rich air mass with tropospheric CO concentrations. The most successful single tracer in this work appears to be θ_w, a meteorological tracer; on the first flight (A315), when measurements were taken ahead of the warm front of a young baroclinic wave, gradients in chemical tracers coincided closely with those in θ_w. Air from three WCBs was sampled during this flight; one originating over the eastern Pacific; a second associated with a developing baroclinic wave over the eastern Atlantic, and a third, in a similar location, associated with a mature low-pressure system. Each had its own distinct signature with the first and third characterized by low ozone, CO, and NO_y concentrations consistent with their low-latitude maritime origins.

The second flight (A325) studied a more mature system, which had started to occlude. It revealed a more complex structure, with the chemical measurements distinguishing more structure than θ_w. Both a WCB and a dry intrusion were sampled during this flight. Thin layers with stratospheric characteristics (enhanced ozone, NO_y and stability, reduced CO and humidity) persisted at the edges of the dry intrusion at least 2½ days after the air was in the vicinity of a tropopause fold. This underlines the significant potential that measurement of trace species offer as tools for understanding the history and nature of conveyor belts which determine not only the cloud and precipitation distributions, but also the structure and evolution of cyclones.

Meteorological interpretation of chemical measurements presented in this paper has relied mainly on trajectory calculations, based on assimilated data fields from the U.K. Meteorological Office operational forecast model. Remarkably good agreement was found in most cases between the chemical air mass characteristics and trajectory end points, particularly for the first flight where there was less fine-scale structure in the aircraft profile. This attests to the fact that the model assimilation had correctly captured the basic structure of the frontal systems studied. The value of combining chemical measurements with trajectory calculations can be seen for the air above the front in Figure 5, which clearly shows two different air masses above and below 6 km. The trajectories were able to distinguish distinctive origins for these two air masses, one of which could be related to an earlier warm conveyor belt over the Pacific.

We have shown that dedicated aircraft flights with chemical instrumentation can reveal structures that are of interest to meteorologists as well as chemists. Clearly, further case studies are needed to establish the variety in chemical signatures of conveyor belts, which are obviously dependent on the geographical origin of these flows. Such studies should also attempt to quantify the transfer of air (and ozone) from the boundary layer to the free troposphere during the lifetime of a typical cyclone, thus establishing the magnitude of their contribution to the ozone budget of the free troposphere. Chemical measurements could also be a valuable input to meteorological models, revealing detailed differences between air masses.

Acknowledgements. We thank the Natural Environment Research Council (NERC) Satellite Station, University of Dundee for the satellite images. S.B. held a CASE studentship jointly supported by NERC and the U.K. Meteorological Office. OCTA was funded by the CEC Environment program.

References

Banic, C.M., G.A. Isaac, H.R. Cho, and J.V. Iribane, The distribution of pollutants near a frontal surface: A comparison between field experiment and modelling, *Water Air Soil Pollut.*, *30*, 171-177, 1986.

Beekmann, M., G. Ancellet, and G. Mégie, Climatology of tropospheric ozone in southern Europe and its relation to potential vorticity, *J. Geophys. Res.*, *99*, 12841-12853, 1994.

Bolton, D., The computation of equivalent potential temperature, *Mon. Weather Rev.*, *108*, 1046-1053, 1980.

Browell, E.V., et al., Large-scale air mass characteristics observed over western Pacific during summertime, *J. Geophys. Res.*, *101*, 1691-1712, 1996.

Brown, R.M., P H Daum, S.E. Schwartz, and M.R. Hjelmfelt, Variations in the chemical composition of clouds during frontal passage, in *The Meteorology of Acid Deposition*, edited by P.J. Samson, pp. 202-212, Air Pollut. Control Assoc., Pittsburgh, Pa., 1984.

Browning, K.A., Organization of clouds and precipitation in extratropical cyclones, in *Extratropical Cyclones - The Erik Palmén Memorial Volume*, Am. Meteorol. Soc., 1990.

Browning, K.A., and B.W. Golding, Mesoscale aspects of a dry intrusion within a vigorous cyclone, *Q. J. R Meteorol. Soc*, *121*, 463-493, 1995

Browning, K.A., and F.F. Hill, Mesoscale analysis of a polar trough interacting with a polar front, *Q. J. R. Meteorol. Soc.*, *111*, 445-462, 1985

Browning, K A , and G. A Monk, A simple model for the synoptic analysis of cold fronts, *Q. J R Meteorol. Soc.*, *108*, 435-452, 1982.

Browning, K.A., and C W. Pardoe, Structure of low-level jet streams ahead of mid-latitude cold fronts, *Q J. R. Met. Soc.*, 99, 619-638, 1973.

Browning, K.A., and N.M Roberts, Structure of a frontal cyclone, *Q. J. R. Meteorol Soc.*, *120*, 1535-1557, 1994.

Carlson, T N., Airflow through midlatitude cyclones and the comma cloud pattern, *Mon. Weather. Rev.*, *108*, 1498-1509, 1980.

Carlson, T N., *Mid-Latitude Weather Systems*, HarperCollins, New York, 1991.

Chatfield, R B , and P J. Crutzen, Sulfur dioxide in remote oceanic air Cloud transport of reactive precursors, *J. Geophys. Res.*, *89*, 7111-7132, 1984.

Chaumerliac, N., R Rosset, M. Renard, and E.C. Nickerson, The transport and redistribution of atmospheric gases in regions of frontal rain, *J. Atmos. Chem* , *14*, 43-51, 1992.

Cho, H.R , M Niewiadomski, J V Iribarne, and O. Melo, A model of the effect of cumulus clouds on the redistribution and transformation of pollutants, *J. Geophys Res.*, *94*, 12895-12910, 1989

Fahey, D.W., et al., In situ observations of NO_y, O_3 and the NO_y/O_3 ratio in the lower stratosphere, *Geophys. Res. Lett.*, *23*, 1653-1656, 1996.

Fishman, J , V. Ramanathan, P.J Crutzen, and S.C. Liu, Tropospheric ozone and climate, *Nature*, *282*, 818-820, 1979

Freeman, M.H., Fronts investigated by the Meteorological Research Flight, *Meteorol Mag.*, *90*, 189-203, 1961

Galloway, J.L., The three-front model: Its philosophy, nature, construction and use, *Weather*, *13*, 3-10, 1958.

Gerbig, C , D. Kley, A. Volz-Thomas, J. Kent, K. Dewey, and D.S. McKenna, Fast-response resonance fluorescence CO measurements aboard the C-130: Instrument characterization and measurements made during NARE 1993, *J. Geophys. Res.*, *101*, 29317-29327, 1996.

Gimson, N.R., Dispersion and removal of pollutants during the passage of an atmospheric frontal system, *Q. J R. Meteorol. Soc.*, *120*, 139-160, 1994

Godson, W.L., Synoptic properties of frontal surfaces, *Q. J. R. Meteorol. Soc.*, *77*, 633-653, 1951

Harrold, T.W., Mechanisms influencing the distribution of precipitation within baroclinic disturbances, *Q J. Roy Meteorol Soc* , *99*, 232-251, 1973

Hegg, D.A., S.A. Rutledge, and P.V. Hobbs, A numerical model for sulfur chemistry in warm frontal rainbands, *J. Geophys. Res* , *89*, 7133-7147, 1984.

Holton, J.R., P.H. Haynes, M.E. McIntyre, A.R Douglass, R.B. Rood, and L. Pfister, Stratosphere-troposphere exchange, *Rev. Geophys.*, *33*(4), 403-439, 1995.

Kavassalis, T.A , O.T Melo, J.V. Iribarne, and H.R. Cho, Cloud microphysics and acid rain formation in frontal circulations, in *Meteorology of Acid Deposition*, edited by J. Laznow and G.J. Stensland, pp. 278-301, Air Pollut. Control Assoc., Pittsburgh, Pa., 1986.

Kuo, Y.-H., R.J. Reed, and S. Low-Nam, Thermal structure and airflow in a model simulation of an occluded marine cyclone, *Mon. Weather. Rev.*, *120*, 2280-2297, 1992.

Kurz, M., Synoptic-scale waves, in *Images in Weather Forecasting*, edited by M.J. Bader et al., pp. 187-205, Cambridge Univ Press, New York, 1995.

Levy, H , II, Normal atmosphere: Large radical and formaldehyde concentrations predicted, *Science*, *173*, 141-143, 1971.

McKenna, D. S., C. J. Hord, and J. M. Kent. Hydroxyl radical concentrations and Kuwait oil fire emission rates for March 1991, *J. Geophys. Res.*, *100*, 26005-26025, 1995.

Murphy, D. M., D. W. Fahey, M. H. Proffitt, S C. Liu, K. R. Chan, C. S. Eubank, S. R Kawa, and K. K. Kelly, Reactive nitrogen and its correlation with ozone in the lower stratosphere and upper troposphere, *J Geophys. Res.*, *98*, 8751-8774, 1993.

Nicholls, S., Measurement of turbulence by an instrumented aircraft in a convective atmospheric boundary layer over the sea, *Q. J. R. Meteorol. Soc.*, *104*, 653-676, 1978.

Niewiadomski, M., A passive pollutant in a three-dimensional field of convective clouds: Numerical simulations, *Atmos. Environ.*, *20*, 139-145, 1986.

Penner, C.M., A three-front model for synoptic analyses, *Q J. R Meteorol. Soc.*, *81*, 89-91, 1955.

Pickering, K E., R.R. Dickerson, G.J. Huffman, J.F. Boatman, and A Schanot, Trace gas transport in the vicinity of frontal convective clouds, *J. Geophys. Res.*, *93*, 759-773, 1988.

Pickering, K.E., et al., Convective transport of biomass burning emissions over Brazil during TRACE A, *J. Geophys Res* , *101*, 23993-24012, 1996.

Ramanathan, V., and R.E. Dickinson, The role of stratospheric ozone in the zonal and seasonal radiation energy balance of the Earth troposphere system, *J. Atmos. Sci.*, *36*, 1084-1104, 1979

Ritter, J.A., The determination of cloud base mass flux and the vertical redistribution of a conservative tracer, in *The Meteorology of Acid Deposition*, edited by P.J. Samson, pp. 177-188, Air Pollut. Control Assoc., Pittsburgh, Pa , 1984.

Schultz, D M., and C.F. Mass, The occlusion process in a midlatitude cyclone over land, *Mon. Weather Rev.*, *121*, 918-940, 1993.

Sturman, A.P., and H.A McGowan, An assessment of boundary-layer air mass characteristics associated with topographically-induced local wind systems, *Boundary Layer Meteorol.*, *74*, 181-193, 1995

Wallace, J. M., and P. V. Hobbs. *Atmospheric Science· An Introductory Survey*, Academic Press, San Diego, Calif , 1997

Weller, R., R. Lilishkis, O. Schrems, R. Neuber, and S. Wessel, Vertical ozone distribution in the marine atmosphere over the central Atlantic Ocean (56°S-50°N), *J. Geophys. Res.*, *101*, 1387-1399, 1996.

Wernli, H., A Lagrangian-based analysis of extratropical cyclones, II, A detailed case study, *Q. J. R. Meteorol. Soc* , *123*, 1677-1707, 1997

Wernli, H. and H.C Davies, A Lagrangian-based analysis of extratropical cyclones, I, The method and some applications, *Q. J. R. Meteorol. Soc.*, *123*, 467-490, 1997.

Wickham, P.G., The practice of weather forecasting, Her Majesty's Stn. Off., Norwich, England, 1970.

Wild, O., K. S. Law, D. S. McKenna, B. J. Bandy, S. A. Penkett, and J A. Pyle, Photochemical trajectory modeling of studies of the North Atlantic region during August 1993, *J. Geophys. Res.*, *101*, 29269-29288, 1996.

Young, M.V., G.A. Monk and K.A. Browning, Interpretation of satellite imagery of a rapidly deepening cyclone, *Q. J. R. Meteorol. Soc.*, *113*, 1089-1115, 1987.

S. Bethan and G. Vaughan, Department of Physics, University of Wales, Aberystwyth SY23 , Wales, U.K. (e-mail: gxv@aber.ac.uk)

C. Gerbig and A. Volz-Thomas, Institut für Chemie und Dynamik der Geosphäre (ICG-2), Forschungszentrum, Jülich, D-52425 Jülich, Germany.

H. Richer and D.A. Tiddeman, Meteorological Research Flight, U.K. Meteorological Office, DRA Farnborough, Hampshire GU14 6TD, England, U.K.

(Received March 20, 1997; revised February 3, 1998; accepted February 12, 1998.)